

# **Build Many Layer Graphene-MoSe<sub>2</sub>-hBN heterojunction with LatticeMixer and VESTA**



By

**Tanvir Ahmad**

Reg. No. 2019-GU-3540

**Habiba Saleem**

Reg. No. 2019-GU-3539

**Rimsha Imtiaz**

Reg. No. 2019-GU-3491

Supervisor

**Dr. M. Rashid**

Associate Professor

Department of Physics

Ghazi University, D.G. Khan

Co-Supervisor

**M. Waqas Nafees**

Lecturer

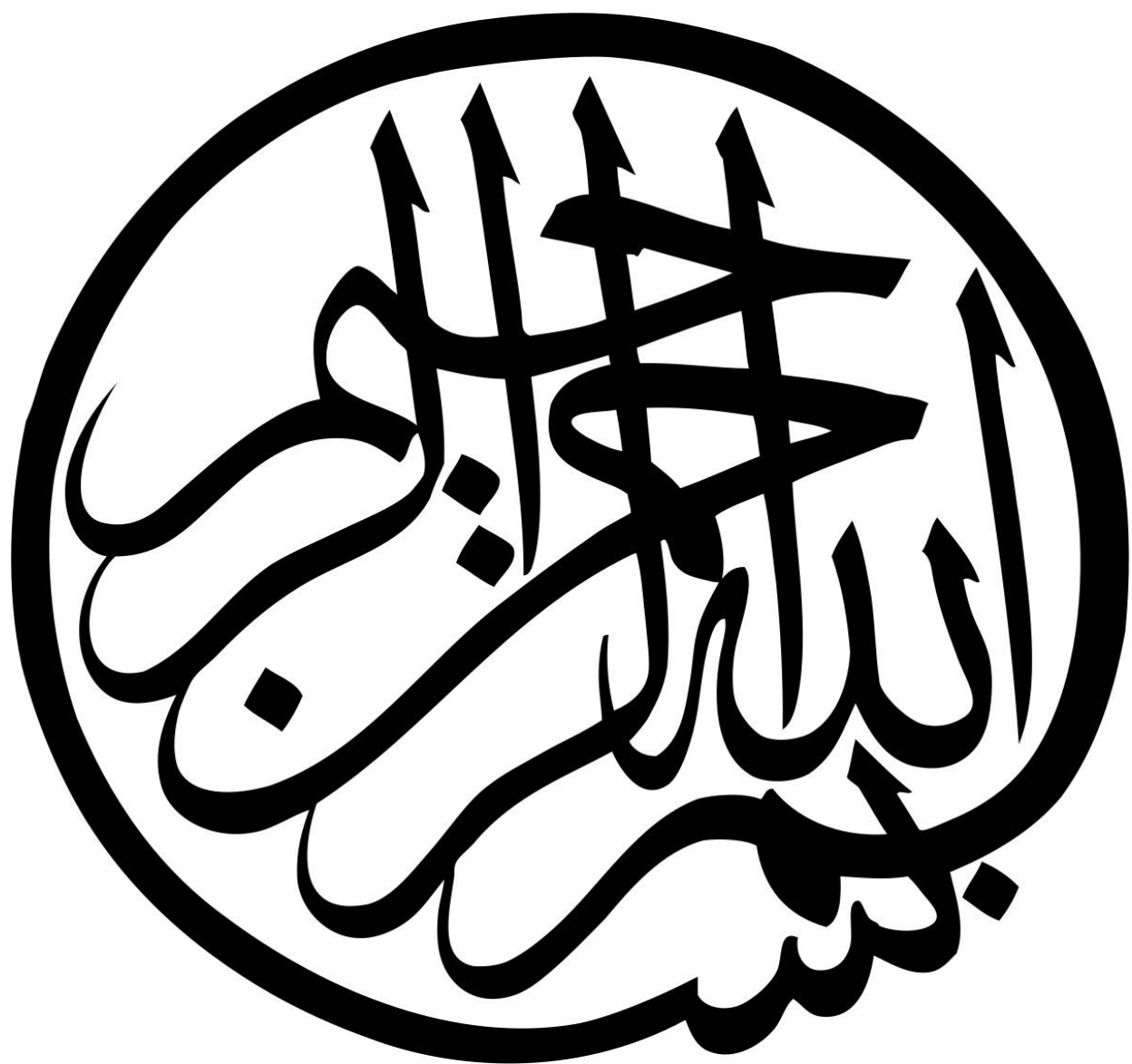
Department of Physics

Ghazi University, D.G. Khan

**Department of Physics**

**Faculty of Sciences**

**Ghazi University, D.G. Khan**



## DECLARATION OF ORIGINALITY

We, **Tanvir Ahmad** registration no.2019-GU-3540, **Habiba Saleem** registration no.2019-GU-3539 and **Rimsha Imtiaz** registration no. 2019-GU-3491 hereby declared that the work presented in the project report entitled “**Build Many Layer Graphene-MoSe<sub>2</sub>-hBN heterojunction with LatticeMixer and VESTA**” in partial fulfillment of BS Degree in Physics from Ghazi University, D.G. Khan. It is our own work and has not submitted as research project report in any form in any other university or institutions in Pakistan.

---

**Tanvir Ahmad**

Reg. No. 2019-GU-3540

---

**Habiba Saleem**

Reg. No. 2019-GU-3539

---

**Rimsha Imtiaz**

Reg. No. 2019-GU-3491

## **FORWARDING SHEET BY RESEARCH SUPERVISOR**

The project report entitled “**Build Many Layer Graphene-MoSe<sub>2</sub>-hBN heterojunction with LatticeMixer and VESTA**” submitted by **Tanvir Ahmad** registration no. 2019-GU-3540, **Habiba Saleem** registration no. 2019-GU-3539 and **Rimsha Imtiaz** registration no. 2019-GU-3491 is partial fulfillment of BS Degree in Physics has been completed under my guidance and supervision. I am satisfied with the quality of research work of student and allow them to submit this project report for further process to graduate with Master of Science degree from Department of Physics, as per GU rules and regulations.

---

**Dr. M. Rashid**

Associate Professor  
Supervisor

---

**M. Waqas Nafees**

Lecturer  
Co-Supervisor

## FINAL APPROVAL

It is certified that the work presented in this project report entitled “**Build Many Layer Graphene-MoSe<sub>2</sub>-hBN heterojunction with LatticeMixer and VESTA**” by **Tanvir Ahmad** registration No. 2019-GU-3540, **Habiba Saleem** registration No. 2019-GU-3539 and **Rimsha Imtiaz** registration No. 2019-GU-3491, fulfill the requirements for award of **Degree of BS Physics** from Department of Physics, Ghazi University, D.G. Khan, Punjab, Pakistan.

Viva Voce Committee

**Chairman**

**Associate Professor**

**(Dr. M Rashid)**

\_\_\_\_\_

**Co-Supervisor**

**Lecturer**

**(M. Waqas Nafees)**

\_\_\_\_\_

**External Examiner**

**Associate Professor**

**(Dr. Fayyaz Hussain**

-----

## ACKNOWLEDGEMENTS

We have no words to express our deepest gratitude to **Allah Almighty** for all of his countless blessings. We owe our deepest respect to most noble messenger **Hazrat Muhammad (P.B.U.H)**, who is forever a torch of guidance and knowledge for all humanity. By virtue of his blessings today we are able to complete our research work and Bachelor of Science in Physics.

The **Almighty Allah** has blessed us through the people who have contributed to the completion of this project. The persons who worth mentioning in our respected research supervisor **Dr. M. Rashid, M. Waqas Nafees and Nadeem Ahmed Qaisrani** who guided and supported us during our whole research work. They are an inspiring personality for us in all fields specially education. Under their supervision from the preliminary to the concluding level enabled us to develop an understanding of the field.

Moreover, we would like to express our sincere thanks to all of our teachers of Physics Department, Ghazi University, D.G. Khan and especially to Chairman **Dr. Rashid Khan** for their sincere appreciation, comments and suggestions.

Of course, any acknowledgments would never be completed without expressing gratitude to our **Parents, Sisters and Brothers**. We owe everything to them and words are never enough express our attribution to our **Parents, Sisters and Brothers**. Our achievements in life would never complete without their prayers and support.

**Tanvir Ahmad**

Reg. No. 2019-GU-3540

**Habiba Saleem**

Reg. No. 2019-GU-3539

**Rimsha Imtiaz**

Reg. No. 2019-GU-3491

## **Abstract:**

In our Project” **Build Many Layer Graphene-MoSe<sub>2</sub>-hBN heterojunction with LatticeMixer and VESTA**” we made many layers of **Graphene-MoSe<sub>2</sub>-hBN** . We can identify and calculate the atomic distance of different atoms of Graphen-MoSe<sub>2</sub> or MoSe<sub>2</sub>-hBN . We can calculate the angle, Dihedral angle and Interfacial angle of different atoms of a crystal.

Heterostuctures of Different crystals give information about their physical, Electric, Magnetic and Dielectric Properties. By Mixing lattices of different crystals, the properties of crystals may change.

We can get different results by changing properties of crystals by mixing their lattices or hetrojunctions. A material is made efficient for its usage and applications in the field of science and Technology in our modern world.

In future, we can explore the properties of materials by making their hetrojunctions. We can study the Nano materials and their potential applications in the field of science and technology. We can study the properties of Nano materials e.g Electric, Magnetic, Dielectric and Optical Properties by making their hetrojunction as a Research area. We can explore and define crystal systems of different crystals to study the Nano materials.

# Contents

<b>Graphene.....</b>	<b>1</b>
<b>1.1 What is Graphene? .....</b>	<b>1</b>
<b>1.2 Structure of graphite and its intercalation compounds .....</b>	<b>2</b>
<b>1.3 Full isolation and characterization.....</b>	<b>3</b>
<b>1.4 Exploring commercial applications.....</b>	<b>3</b>
<b>1.5 Structure .....</b>	<b>3</b>
<b>1.6 Bonding .....</b>	<b>4</b>
<b>1.7 Geometry .....</b>	<b>5</b>
<b>1.8 Stability .....</b>	<b>5</b>
<b>1.9 Properties .....</b>	<b>6</b>
<b>1.9.1 Electronic Properties of Graphen.....</b>	<b>6</b>
<b>1.9.2 Electronic Spectrum .....</b>	<b>6</b>
<b>1.9.3 Strong magnetic fields.....</b>	<b>7</b>
<b>1.9.4 Van der Waals force .....</b>	<b>7</b>
<b>1.9.5 'Massive' electrons .....</b>	<b>7</b>
<b>1.9.6 Permittivity .....</b>	<b>8</b>
<b>1.9.7 Optical .....</b>	<b>8</b>
<b>1.9.8 Spin transport .....</b>	<b>9</b>
<b>1.10 Magnetic properties.....</b>	<b>9</b>
<b>1.10.1 Strong magnetic fields.....</b>	<b>9</b>
<b>1.10.2 Magnetic substrates .....</b>	<b>9</b>
<b>1.10.3 Thermal conductivity .....</b>	<b>10</b>
<b>1.11 Mechanical .....</b>	<b>11</b>
<b>1.12 Forms .....</b>	<b>12</b>
<b>1.12.1 Monolayer sheets.....</b>	<b>12</b>
<b>1.12.2 Bilayer graphene .....</b>	<b>13</b>



1.12.3 Graphene superlattices .....	13
1.13 Graphene nanoribbons .....	14
1.14 Graphene oxide .....	15
1.15 3D graphene .....	16
1.16 Reinforced graphene.....	17
1.17 Applications .....	17
1.18 Potential applications.....	17
1.19 Graphene products .....	18
1.20 Molybdenum diselenide (MoSe <sub>2</sub> ) .....	20
1.20.1 Structure.....	20
1.20.2 Synthesis .....	21
2D-MoSe <sub>2</sub> .....	21
1.20.3 Natural occurrence.....	21
1.21 HEXAGONAL BORON NITRIDE (HBN) POWDER.....	23
1.21.1 Characteristic Of Hexagonal Boron Nitride Powder .....	25
1.21.2 Physical Properties Of Hexagonal Boron Nitride (HBN) Powder .....	25
1.21.3 Structural and Electronic Properties of BN .....	25
1.21.4 Uses Of Hex Boron Nitride (HBN) Powder .....	26
Materials & Methodology .....	32
VESTA.....	32
2.1 Introduction .....	32
2.2 New features in VESTA.....	32
2.3 Circumstances behind the development of VESTA .....	33
2.4 Basics: .....	34
2.4.1 Symmetry and Unit Cell .....	34
2.4.2 Crystal systems and space groups .....	34
2.5 General features.....	35

2.5.1 Cross-platform software .....	35
2.5.2 Scalable.....	35
2.5.3 Multiple windows and tabs .....	35
2.5.4 Smart ways of drawing boundary specification .....	36
2.6 Dealing with structural models .....	36
2.6.1 Visualization of structural models.....	36
2.7 Functions in VESTA:.....	37
2.7.1 Transformation of the unit cell .....	37
2.7.2 Creation of superstructures and substructures.....	38
2.7.3 Magnetic Structures.....	39
2.7.4 OVERLAYING MULTIPLE DATA.....	40
2.7.5 Making Hetrojunction: .....	41
2.7.6 Making Heterostructures.....	42
2.7.7 Making Monolayers-Many Layers .....	43
2.7.8 Supercells .....	44
2.7.9 Nanorods .....	44
2.8 Display crystallographic information.....	45
2.9 Lattice transformation.....	45
2.10 Vectors on atoms .....	45
2.11 Dealing with volumetric data: .....	46
2.12 Visualization of volumetric data.....	46
2.13 Surface coloring .....	46
2.14 Peak search .....	47
2.15 Display lattice planes .....	47
2.17 Main Features:.....	47
2.17.1Visualization of Crystal Morphologies .....	47
2.17.2 Collaboration with external programs .....	47

<b>2.17.3 STRUCTURE TIDY .....</b>	<b>48</b>
<b>2.17.4 RIETAN-FP .....</b>	<b>48</b>
<b>2.17.5 MADEL .....</b>	<b>48</b>
<b>2.18 Screenshots .....</b>	<b>48</b>
<b>2.19 Crystal structure .....</b>	<b>49</b>
<b>Results and Discussion: .....</b>	<b>50</b>
<b>Conclusion: .....</b>	<b>54</b>

## List of Figures:

Figure1.1.....	2
Figure 1.2.....	4.
Figure 1.3.....	4
Figure 1.4.....	5
Figure 1.5.....	6
Figure 1.6.....	14
Figure 1.7.....	14
Figure 1.8.....	15
Figure 1.9.....	17
Figure 1.10.....	18
Figure 1.11 .....	19
Figure 1.12.....	19
Figure 1.13.....	20
Figure 1.14.....	22
Figure 1.15.....	22
Figure 1.16.....	24
Figure 1.17.....	24
Figure 2.1 .....	34
Figure 2.2.....	35
Figure 2.4.....	36
Figure2.5.....	36
Figure 2.6.....	36

Figure 2.7.....	36
Figure 2.8.....	36
Figure 2.9.....	37
Figure 2.10.....	37
Figure 2.11.....	37
Figure 2.12.....	38
Figure 2.13.....	39
Figure 2.14.....	40
Figure 2.15.....	41
Figure 2.16.....	41
Figure 2.17.....	42
Figure 2.18.....	43
Figure 2.19.....	43
Figure 2.20.....	43
Figure 2.21.....	44
Figure 2.22.....	44
Figure 2.23.....	44
Figure 2.24.....	46
Figure2.25.....	46
Figure 2.26.....	47
Figure 2.27.....	49
Figure 3.1.....	50
Figure 3.2.....	50
Figure 3.3.....	51
Figure 3.4.....	51
Figure 3.5.....	51
Figure 3.6.....	51
Figure 3.7.....	52
Figure 3.8.....	52
Figure3.9.....	53
Figure3.10.....	53

**List of Tables**

Table 1.1 ..... 22

Table 1.2 ..... 22

Table 1.3 ..... 23

Table 1.4 ..... 23

## Chapter no.1 Introduction

### Graphene

#### 1.1 What is Graphene?

Graphene is a one-atom-thick layer of carbon atoms arranged in a hexagonal lattice. It is the building-block of Graphite (which is used, among others things, in pencil tips), but graphene is a remarkable substance on its own - with a multitude of astonishing properties which repeatedly earn it the title wonder material.

**Graphene** is an allotrope of carbon consisting of a single layer of atoms arranged in a hexagonal lattice nanostructure. The name is derived from "graphite" and the suffix -ene, reflecting the fact that the graphite allotrope of carbon contains numerous double bonds.

Each atom in a graphene sheet is connected to its three nearest neighbors by a strong  $\sigma$ -bond, and contributes to a valence band one electron that extends over the whole sheet. This is the same type of bonding seen in carbon nanotubes and polycyclic aromatic hydrocarbons, and (partially) in fullerenes and glassy carbon[1]. The valence band is touched by a conduction band, making graphene a semimetal with unusual electronic properties that are best described by theories for massless relativistic particles[2]. Charge carriers in graphene show linear, rather than quadratic, dependence of energy on momentum, and field-effect transistors with graphene can be made that show bipolar conduction. Charge transport is ballistic over long distances; the material exhibits large quantum oscillations and large and nonlinear diamagnetism. Graphene conducts heat and electricity very efficiently along its plane. The material strongly absorbs light of all visible wavelengths, which accounts for the black color of graphite; yet a single graphene sheet is nearly transparent because of its extreme thinness. The material is about 100 times as strong as would be the strongest steel of the same thickness.

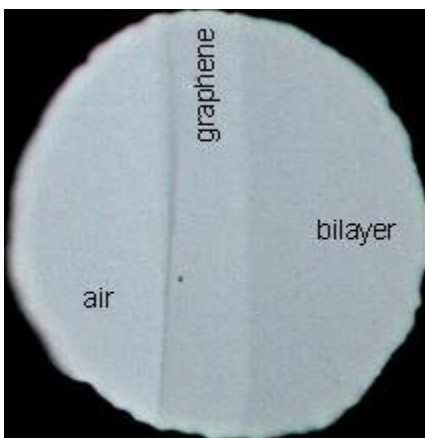


**Fig.1.1 Photograph of a suspended graphene membrane in transmitted light. This one-atom-thick material can be seen with the naked eye because it absorbs approximately 2.3% of light.**

Scientists theorized the potential existence and production of graphene for decades. It has likely been unknowingly produced in small quantities for centuries, through the use of pencils and other similar applications of graphite. It was possibly observed in electron microscopes in 1962, but studied only while supported on metal surfaces.

## **1.2 Structure of graphite and its intercalation compounds**

In 1859, Benjamin Brodie noted the highly lamellar structure of thermally reduced graphite oxide. In 1916, Peter Debye and Paul Scherrer determined the structure of graphite by powder X-ray diffraction. The structure was studied in more detail by V. Kohlschütter and P. Haenni in 1918, who also described the properties of graphite oxide paper[3]. Its structure was determined from single-crystal diffraction in 1924.

The theory of graphene was first explored by P. R. Wallace in 1947 as a starting point for understanding the electronic properties of 3D graphite. The emergent massless Dirac equation was first pointed out in 1984 separately by Gordon Walter Semenoff and by David P. DiVincenzo and Eugene J. Mele. Semenoff emphasized the occurrence in a magnetic field of an electronic Landau level precisely at the Dirac point. This level is responsible for the anomalous integer quantum Hall effect.

### **1.3 Full isolation and characterization**

Andre Geim and Konstantin Novoselov at the Nobel Laureate press conference, Royal Swedish Academy of Sciences, 2010.

Graphene was properly isolated and characterized in 2004 by Andre Geim and Konstantin Novoselov at the University of Manchester[4]. They pulled graphene layers from graphite with a common adhesive tape in a process called either micromechanical cleavage or the Scotch tape technique.<sup>[46]</sup> The graphene flakes were then transferred onto thin silicon dioxide (silica) layer on a silicon plate ("wafer"). The silica electrically isolated the graphene and weakly interacted with it, providing nearly charge-neutral graphene layers. The silicon beneath the SiO could be used as a "back gate" electrode to vary the charge density in the graphene over a wide range.

This work resulted in the two winning the Nobel Prize in Physics in 2010 "for groundbreaking experiments regarding the two-dimensional material graphene. Their publication, and the surprisingly easy preparation method that they described, sparked a "graphene gold rush". Research expanded and split off into many different subfields, exploring different exceptional properties of the material—quantum mechanical, electrical, chemical, mechanical, optical, magnetic, etc.

### **1.4 Exploring commercial applications**

Since the early 2000s, a number of companies and research laboratories have been working to develop commercial applications of graphene. In 2014 a National Graphene Institute was established with that purpose at the University of Manchester, with a 60 million GBP initial funding[5]. In North East England two commercial manufacturers, Applied Graphene Materials and Thomas Swan Limited have begun manufacturing. Cambridge Nanosystems is a large-scale graphene powder production facility in East Anglia.

### **1.5 Structure**

Graphene is a single layer (monolayer) of carbon atoms, tightly bound in a hexagonal honeycomb lattice. It is an allotrope of carbon in the form of a plane of sp<sup>2</sup>-bonded atoms with a molecular bond length of 0.142 nanometres.



## 1.6 Bonding

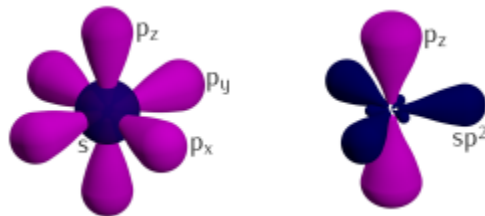


**Fig.1.2 Sp-Hybridization**

Carbon orbitals  $2s$ ,  $2p_x$ ,  $2p_y$  form the hybrid orbital  $sp^2$  with three major lobes at  $120^\circ$ . The remaining orbital,  $p_z$ , is sticking out of the graphene's plane.

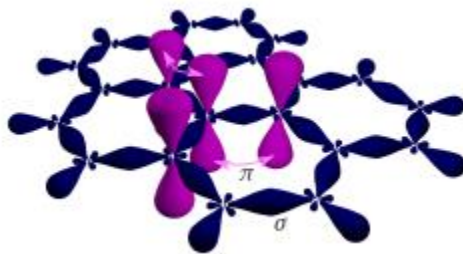


**Fig.1.3 sigma & pi bonds**

Sigma and pi bonds in graphene. Sigma bonds result from an overlap of  $sp^2$  hybrid orbitals, whereas pi bonds emerge from tunneling between the protruding  $p_z$  orbitals.

Three of the four outer-shell electrons of each atom in a graphene sheet occupy three  $sp^2$  hybrid orbitals – a combination of orbitals  $s$ ,  $p_x$  and  $p_y$  — that are shared with the three nearest atoms, forming  $\sigma$ -bonds. The length of these bonds is about 0.142 nanometers.

The remaining outer-shell electron occupies a  $p_z$  orbital that is oriented perpendicularly to the plane. These orbitals hybridize together to form two half-filled bands of free-moving electrons,  $\pi$  and  $\pi^*$ , which are responsible for most of graphene's notable electronic properties. Recent quantitative estimates of aromatic stabilization and limiting size derived from the enthalpies of hydrogenation ( $\Delta H_{\text{hydro}}$ ) agree well with the literature reports.

Graphene sheets stack to form graphite with an interplanar spacing of 0.335 nm (3.35 Å).

Graphene sheets in solid form usually show evidence in diffraction for graphite's (002) layering. This is true of some single-walled nanostructures[6]. However, unlayered graphene with only (hk0) rings has been found in the core of presolar graphite onions[7]. TEM studies show faceting

at defects in flat graphene sheets and suggest a role for two-dimensional crystallization from a melt.

## 1.7 Geometry

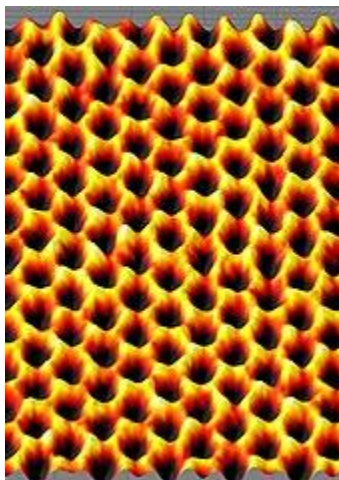


**Fig 1.4 Scanning probe microscopy image of graphene**

The hexagonal lattice structure of isolated, single-layer graphene can be directly seen with transmission electron microscopy (TEM) of sheets of graphene suspended between bars of a metallic grid. Some of these images showed a "rippling" of the flat sheet, with amplitude of about one nanometer. These ripples may be intrinsic to the material as a result of the instability of two-dimensional crystals, or may originate from the ubiquitous dirt seen in all TEM images of graphene. Photoresist residue, which must be removed to obtain atomic-resolution images, may be the "adsorbates" observed in TEM images, and may explain the observed rippling.

The hexagonal structure is also seen in scanning tunneling microscope (STM) images of graphene supported on silicon dioxide substrates[9]. The rippling seen in these images is caused by conformation of graphene to the substrate's lattice, and is not intrinsic.

## 1.8 Stability

Ab initio calculations show that a graphene sheet is thermodynamically unstable if its size is less than about 20 nm and becomes the most stable fullerene (as within graphite) only for molecules larger than 24,000 atoms.

## 1.9 Properties

### 1.9.1 Electronic Properties of Graphene

Electronic band structure of graphene. Valence and conduction bands meet at the six vertices of the hexagonal Brillouin zone and form linearly dispersing Dirac cones.

Graphene is a zero-gap semiconductor, because its conduction and valence bands meet at the Dirac points. The Dirac points are six locations in momentum space, on the edge of the Brillouin zone, divided into two non-equivalent sets of three points [10]. The two sets are labeled K and K'. The sets give graphene a valley degeneracy of  $g_v = 2$ . By contrast, for traditional semiconductors the primary point of interest is generally  $\Gamma$ , where momentum is zero. Four electronic properties separate it from other condensed matter systems.

However, if the in-plane direction is no longer infinite, but confined, its electronic structure would change. They are referred to as graphene nanoribbons. If it is "zig-zag", the bandgap would still be zero. If it is "armchair", the bandgap would be non-zero.

Graphene's hexagonal lattice can be regarded as two interleaving triangular lattices. This perspective was successfully used to calculate the band structure for a single graphite layer using a tight-binding approximation.

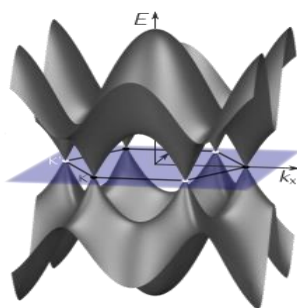


**Fig. 1.5 Electric effect**

### 1.9.2 Electronic Spectrum

Electrons propagating through graphene's honeycomb lattice effectively lose their mass, producing quasi-particles that are described by a 2D analogue of the Dirac equation rather than the Schrödinger equation for spin-1/2 particles[11].

### 1.9.3 Strong magnetic fields

In magnetic fields above 10 tesla or so additional plateaus of the Hall conductivity at  $\sigma_{xy} = \nu e^2/h$  with  $\nu = 0, \pm 1, \pm 4$  are observed. A plateau at  $\nu = 3$  and the fractional quantum Hall effect at  $\nu = 1/3$  were also reported[12].

These observations with  $\nu = 0, \pm 1, \pm 3, \pm 4$  indicate that the four-fold degeneracy (two valley and two spin degrees of freedom) of the Landau energy levels is partially or completely lifted.

### 1.9.4 Van der Waals force

The Van der Waals force (or dispersion force) is also unusual, obeying an inverse cubic, asymptotic power law in contrast to the usual inverse quartic.

### 1.9.5 'Massive' electrons

Graphene's unit cell has two identical carbon atoms and two zero-energy states: one in which the electron resides on atom A, the other in which the electron resides on atom B. However, if the two atoms in the unit cell are not identical, the situation changes. Hunt et al. show that placing hexagonal boron nitride (h-BN) in contact with graphene can alter the potential felt at atom A versus atom B enough that the electrons develop a mass and accompanying band gap of about 30 meV [0.03 Electron Volt(eV)].

The mass can be positive or negative. An arrangement that slightly raises the energy of an electron on atom A relative to atom B gives it a positive mass, while an arrangement that raises the energy of atom B produces a negative electron mass. The two versions behave alike and are indistinguishable via optical spectroscopy. An electron traveling from a positive-mass region to a negative-mass region must cross an intermediate region where its mass once again becomes zero. This region is gapless and therefore metallic. Metallic modes bounding semiconducting regions of opposite-sign mass is a hallmark of a topological phase and display much the same physics as topological insulators.

If the mass in graphene can be controlled, electrons can be confined to massless regions by surrounding them with massive regions, allowing the patterning of quantum dots, wires, and other mesoscopic structures. It also produces one-dimensional conductors along the boundary. These wires would be protected against backscattering and could carry currents without dissipation.

### 1.9.6 Permittivity

Graphene's permittivity varies with frequency. Over a range from microwave to millimeter wave frequencies it is roughly 3.3. This permittivity, combined with the ability to form both conductors and insulators, means that theoretically, compact capacitors made of graphene could store large amounts of electrical energy.

### 1.9.7 Optical

Graphene's unique optical properties produce an unexpectedly high opacity for an atomic monolayer in vacuum, absorbing  $\pi\alpha \approx 2.3\%$  of light, from visible to infrared. Here,  $\alpha$  is the fine-structure constant. This is a consequence of the "unusual low-energy electronic structure of monolayer graphene that features electron and hole conical bands meeting each other at the Dirac point... [which] is qualitatively different from more common quadratic massive bands." Based on the Slonczewski–Weiss–McClure (SWMcC) band model of graphite, the interatomic distance, hopping value and frequency cancel when optical conductance is calculated using Fresnel equations in the thin-film limit.

Although confirmed experimentally, the measurement is not precise enough to improve on other techniques for determining the fine-structure constant.

Multi-Parametric Surface Plasmon Resonance was used to characterize both thickness and refractive index of chemical-vapor-deposition (CVD)-grown graphene films. The measured refractive index and extinction coefficient values at 670 nm ( $6.7 \times 10^{-7}$  m) wavelength are 3.135 and 0.897, respectively. The thickness was determined as 3.7 Å from a 0.5 mm area, which agrees with 3.35 Å reported for layer-to-layer carbon atom distance of graphite crystals. The method can be further used also for real-time label-free interactions of graphene with organic and inorganic substances. Furthermore, the existence of unidirectional surface plasmons in the nonreciprocal graphene-based gyrotropic interfaces has been demonstrated theoretically. By efficiently controlling the chemical potential of graphene, the unidirectional working frequency can be continuously tunable from THz to near-infrared and even visible. Particularly, the unidirectional frequency bandwidth can be 1–2 orders of magnitude larger than that in metal under the same magnetic field, which arises from the superiority of extremely small effective electron mass in graphene.

Graphene's band gap can be tuned from 0 to 0.25 eV (about 5 micrometre wavelength) by applying voltage to a dual-gate bilayer graphene field-effect transistor (FET) at room temperature. The optical response of graphene nanoribbons is tunable into the terahertz regime by an applied magnetic field. Graphene/graphene oxide systems exhibit electrochromic behavior, allowing tuning of both linear and ultrafast optical properties.

A graphene-based Bragg grating (one-dimensional photonic crystal) has been fabricated and demonstrated its capability for excitation of surface electromagnetic waves in the periodic structure by using 633 nm ( $6.33 \times 10^{-7}$  m) He–Ne laser as the light source.

### **1.9.8 Spin transport**

Graphene is claimed to be an ideal material for spintronics due to its small spin–orbit interaction and the near absence of nuclear magnetic moments in carbon (as well as a weak hyperfine interaction). Electrical spin current injection and detection has been demonstrated up to room temperature. Spin coherence length above 1 micrometre at room temperature was observed, and control of the spin current polarity with an electrical gate was observed at low temperature.

## **1.10 Magnetic properties**

### **1.10.1 Strong magnetic fields**

Spintronic and magnetic properties can be present in graphene simultaneously. Low-defect graphene nanomeshes manufactured by using a non-lithographic method exhibit large-amplitude ferromagnetism even at room temperature. Additionally, a spin pumping effect is found for fields applied in parallel with the planes of few-layer ferromagnetic nanomeshes, while a magnetoresistance hysteresis loop is observed under perpendicular fields.[13]

### **1.10.2 Magnetic substrates**

In 2014 researchers magnetized graphene by placing it on an atomically smooth layer of magnetic yttrium iron garnet. The graphene's electronic properties were unaffected. Prior approaches involved doping graphene with other substances. The dopant's presence negatively affected its electronic properties.

### 1.10.3 Thermal conductivity

Thermal transport in graphene is an active area of research, which has attracted attention because of the potential for thermal management applications. Following predictions for graphene and related carbon nanotubes, early measurements of the thermal conductivity of suspended graphene reported an exceptionally large thermal conductivity up to  $5300 \text{ W}\cdot\text{m}^{-1}\cdot\text{K}^{-1}$ ,<sup>[133]</sup> compared with the thermal conductivity of pyrolytic graphite of approximately  $2000 \text{ W}\cdot\text{m}^{-1}\cdot\text{K}^{-1}$  [14] at room temperature. However, later studies primarily on more scalable but more defected graphene derived by Chemical Vapor Deposition have been unable to reproduce such high thermal conductivity measurements, producing a wide range of thermal conductivities between  $1500 - 2500 \text{ W}\cdot\text{m}^{-1}\cdot\text{K}^{-1}$  for suspended single layer graphene. The large range in the reported thermal conductivity can be caused by large measurement uncertainties as well as variations in the graphene quality and processing conditions. In addition, it is known that when single-layer graphene is supported on an amorphous material, the thermal conductivity is reduced to about  $500 - 600 \text{ W}\cdot\text{m}^{-1}\cdot\text{K}^{-1}$  at room temperature as a result of scattering of graphene lattice waves by the substrate, and can be even lower for few layer graphene encased in amorphous oxide. Likewise, polymeric residue can contribute to a similar decrease in the thermal conductivity of suspended graphene to approximately  $500 - 600 \text{ W}\cdot\text{m}^{-1}\cdot\text{K}^{-1}$  for bilayer graphene

It has been suggested that the isotopic composition, the ratio of  $^{12}\text{C}$  to  $^{13}\text{C}$ , has a significant impact on the thermal conductivity. For example, isotopically pure  $^{12}\text{C}$  graphene has higher thermal conductivity than either a 50:50 isotope ratio or the naturally occurring 99:1 ratio. It can be shown by using the Wiedemann–Franz law, that the thermal conduction is phonon-dominated. However, for a gated graphene strip, an applied gate bias causing a Fermi energy shift much larger than  $k_{\text{B}}T$  can cause the electronic contribution to increase and dominate over the phonon contribution at low temperatures. The ballistic thermal conductance of graphene is isotropic.

Potential for this high conductivity can be seen by considering graphite, a 3D version of graphene that has basal plane thermal conductivity of over a  $1000 \text{ W}\cdot\text{m}^{-1}\cdot\text{K}^{-1}$  (comparable to diamond). In graphite, the c-axis (out of plane) thermal conductivity is over a factor of  $\sim 100$  smaller due to the weak binding forces between basal planes as well as the larger lattice spacing.

In addition, the ballistic thermal conductance of graphene is shown to give the lower limit of the ballistic thermal conductances, per unit circumference, length of carbon nanotubes.

Despite its 2-D nature, graphene has 3 acoustic phonon modes. The two in-plane modes (LA, TA) have a linear dispersion relation, whereas the out of plane mode (ZA) has a quadratic dispersion relation. Due to this, the  $T^2$  dependent thermal conductivity contribution of the linear modes is dominated at low temperatures by the  $T^{1.5}$  contribution of the out of plane mode. Some graphene phonon bands display negative Grüneisen parameters. At low temperatures (where most optical modes with positive Grüneisen parameters are still not excited) the contribution from the negative Grüneisen parameters will be dominant and thermal expansion coefficient (which is directly proportional to Grüneisen parameters) negative. The lowest negative Grüneisen parameters correspond to the lowest transverse acoustic ZA modes. Phonon frequencies for such modes increase with the in-plane lattice parameter since atoms in the layer upon stretching will be less free to move in the z direction. This is similar to the behavior of a string, which, when it is stretched, will have vibrations of smaller amplitude and higher frequency. This phenomenon, named "membrane effect," was predicted by Lifshitz in 1952.

## 1.11 Mechanical

The (two-dimensional) density of graphene is 0.763 mg per square meter.

Graphene is the strongest material ever tested, with an intrinsic tensile strength of 130 GPa (19,000,000 psi) (with representative engineering tensile strength ~50-60 GPa for stretching large-area freestanding graphene) and a Young's modulus (stiffness) close to 1 TPa (150,000,000 psi). The Nobel announcement illustrated this by saying that a 1 square meter graphene hammock would support a 4 kg cat but would weigh only as much as one of the cat's whiskers, at 0.77 mg (about 0.001% of the weight of 1 m<sup>2</sup> of paper).[15]

Large-angle-bent graphene monolayer has been achieved with negligible strain, showing mechanical robustness of the two-dimensional carbon nanostructure. Even with extreme deformation, excellent carrier mobility in monolayer graphene can be preserved.<sup>1</sup>

The spring constant of suspended graphene sheets has been measured using an atomic force microscope (AFM). Graphene sheets were suspended over SiO cavities where an AFM tip was used to apply a stress to the sheet to test its mechanical properties. Its spring constant was in the



range 1–5 N/m and the stiffness was 0.5 TPa, which differs from that of bulk graphite. These intrinsic properties could lead to applications such as NEMS as pressure sensors and resonator. Due to its large surface energy and out of plane ductility, flat graphene sheets are unstable with respect to scrolling, i.e. bending into a cylindrical shape, which is its lower-energy state.

As is true of all materials, regions of graphene are subject to thermal and quantum fluctuations in relative displacement. Although the amplitude of these fluctuations is bounded in 3D structures (even in the limit of infinite size), the Mermin–Wagner theorem shows that the amplitude of long-wavelength fluctuations grows logarithmically with the scale of a 2D structure, and would therefore be unbounded in structures of infinite size. Local deformation and elastic strain are negligibly affected by this long-range divergence in relative displacement. It is believed that a sufficiently large 2D structure, in the absence of applied lateral tension, will bend and crumple to form a fluctuating 3D structure. Researchers have observed ripples in suspended layers of graphene, and it has been proposed that the ripples are caused by thermal fluctuations in the material. As a consequence of these dynamical deformations, it is debatable whether graphene is truly a 2D structure. It has recently been shown that these ripples, if amplified through the introduction of vacancy defects, can impart a negative Poisson's ratio into graphene, resulting in the thinnest auxetic material known so far.

Graphene nanosheets have been incorporated into a Ni matrix through a plating process to form Ni-graphene composites on a target substrate. The enhancement in mechanical properties of the composites is attributed to the high interaction between Ni and graphene and the prevention of the dislocation sliding in the Ni matrix by the graphene.

## **1.12 Forms**

### **1.12.1 Monolayer sheets**

In 2013 a group of Polish scientists presented a production unit that allows the manufacture of continuous monolayer sheets. The process is based on graphene growth on a liquid metal matrix. The product of this process was called High Strength Metallurgical Graphene. In a new study published in Nature, the researchers have used a single layer graphene electrode and a novel surface sensitive non-linear spectroscopy technique to investigate the top-most water layer

at the electrochemically charged surface. They found that the interfacial water response to applied electric field is asymmetric with respect to the nature of the applied field.

### **1.12.2 Bilayer graphene**

Bilayer graphene displays the anomalous quantum Hall effect, a tunable band gap and potential for excitonic condensation making it promising. Bilayer graphene typically can be found either in twisted configurations where the two layers are rotated relative to each other or graphitic Bernal stacked configurations where half the atoms in one layer lie atop half the atoms in the other. Stacking order and orientation govern the optical and electronic properties of bilayer graphene.

One way to synthesize bilayer graphene is via chemical vapor deposition, which can produce large bilayer regions that almost exclusively conform to a Bernal stack geometry.

It has been shown that the two graphene layers can withstand important strain or doping mismatch which ultimately should lead to their exfoliation.

### **1.12.3 Graphene superlattices**

Periodically stacked graphene and its insulating isomorph provide a fascinating structural element in implementing highly functional superlattices at the atomic scale, which offers possibilities in designing nanoelectronic and photonic devices. Various types of superlattices can be obtained by stacking graphene and its related forms. The energy band in layer-stacked superlattices is found to be more sensitive to the barrier width than that in conventional III–V semiconductor superlattices. When adding more than one atomic layer to the barrier in each period, the coupling of electronic wavefunctions in neighboring potential wells can be significantly reduced, which leads to the degeneration of continuous subbands into quantized energy levels. When varying the well width, the energy levels in the potential wells along the L-M direction behave distinctly from those along the K-H direction.

A superlattice corresponds to a periodic or quasi-periodic arrangement of different materials, and can be described by a superlattice period which confers a new translational symmetry to the system, impacting their phonon dispersions and subsequently their thermal transport properties. Recently, uniform monolayer graphene-hBN structures have been successfully synthesized via lithography patterning coupled with chemical vapor deposition (CVD). Furthermore,

superlattices of graphene-hBN are ideal model systems for the realization and understanding of coherent (wave-like) and incoherent (particle-like) phonon thermal transport[16]

## 1.13 Graphene nanoribbons

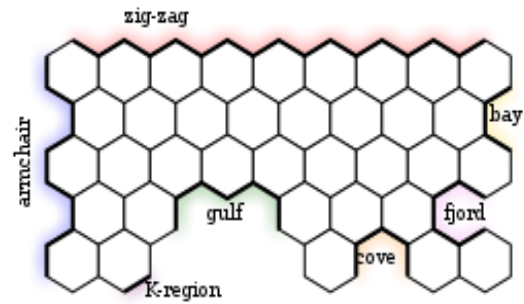


Fig. 1.6 Names for graphene edge topologies

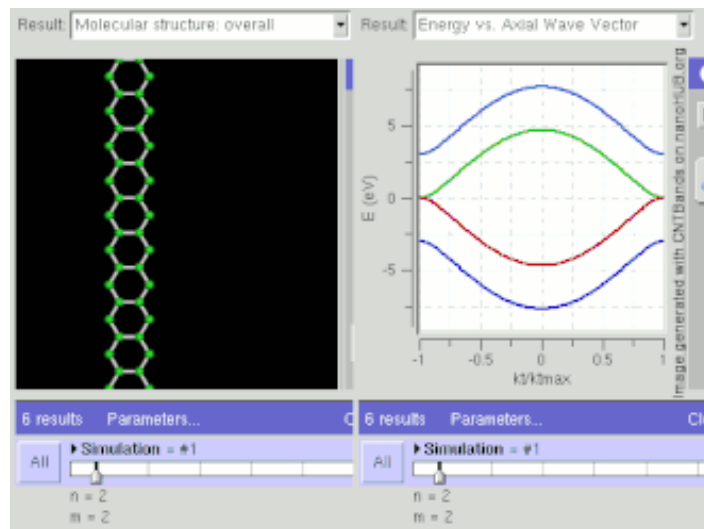
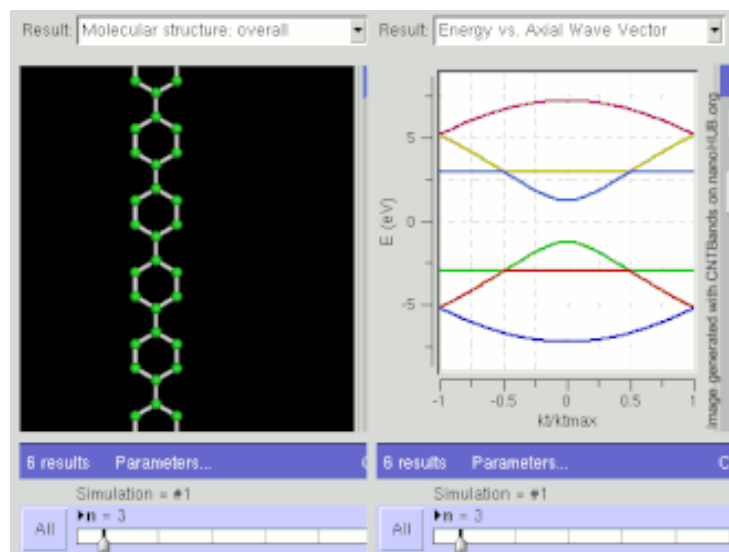


Fig.1.7 GNR Electronic band structure of graphene strips of varying widths in zig-zag orientation. Tight-binding calculations show that they are all metallic.



**Fig.1.8 GNR Electronic band structure of graphene strips of various widths in the armchair orientation. Tight-binding calculations show that they are semiconducting or metallic depending on width (chirality).**

Graphene nanoribbons ("nanostripes" in the "zig-zag"/"zigzag" orientation), at low temperatures, show spin-polarized metallic edge currents, which also suggests applications in the new field of spintronics. (In the "armchair" orientation, the edges behave like semiconductors[17])

## 1.14 Graphene oxide

Graphene oxide is usually produced through chemical exfoliation of graphite. A particularly popular technique is the improved Hummer's method. Using paper-making techniques on dispersed, oxidized and chemically processed graphite in water, the monolayer flakes form a single sheet and create strong bonds. These sheets, called graphene oxide paper, have a measured tensile modulus of 32 GPa. The chemical property of graphite oxide is related to the functional groups attached to graphene sheets. These can change the polymerization pathway and similar chemical processes. Graphene oxide flakes in polymers display enhanced photoconducting properties. Graphene is normally hydrophobic and impermeable to all gases and liquids (vacuum-tight). However, when formed into graphene oxide-based capillary membrane, both liquid water and water vapor flow through as quickly as if the membrane was not present.

In 2022 were performed an evaluation of biological effects of graphene oxide. It was shown the graphene oxide at low doses was evaluated for its biological effects on larvae and the imago of *Drosophila melanogaster*. Oral administration of graphene oxide at concentrations of 0.02-1% has a beneficial effect on the developmental rate and hatching ability of larvae. Long-term administration of a low dose of graphene oxide extends *Drosophila* lifespan and significantly enhances resistance to environmental stresses. These suggest about graphene oxide affects carbohydrate and lipid metabolism in adult *Drosophila*. These findings might provide a useful reference to assess the biological effects of graphene oxide, which could play an important role in a variety of graphene-based biomedical applications.

### **1.15 3D graphene**

In 2013, a three-dimensional honeycomb of hexagonally arranged carbon was termed 3D graphene, and self-supporting 3D graphene was also produced. 3D structures of graphene can be fabricated by using either CVD or solution based methods. A 2016 review by Khurram and Xu et al. provided a summary of then-state-of-the-art techniques for fabrication of the 3D structure of graphene and other related two-dimensional materials. In 2013, researchers at Stony Brook University reported a novel radical-initiated crosslinking method to fabricate porous 3D free-standing architectures of graphene and carbon nanotubes using nanomaterials as building blocks without any polymer matrix as support. These 3D graphene (all-carbon) scaffolds/foams have applications in several fields such as energy storage, filtration, thermal management and biomedical devices and implants.

Box-shaped graphene (BSG) nanostructure appearing after mechanical cleavage of pyrolytic graphite was reported in 2016. The discovered nanostructure is a multilayer system of parallel hollow nanochannels located along the surface and having quadrangular cross-section. The thickness of the channel walls is approximately equal to 1 nm. Potential fields of BSG application include: ultra-sensitive detectors, high-performance catalytic cells, nanochannels for DNA sequencing and manipulation, high-performance heat sinking surfaces, rechargeable batteries of enhanced performance, nanomechanical resonators, electron multiplication channels in emission nanoelectronic devices, high-capacity sorbents for safe hydrogen storage.

Three-dimensional bilayer graphene has also been reported[18]

## 1.16 Reinforced graphene

Graphene reinforced with embedded carbon nanotube reinforcing bars ("rebar") is easier to manipulate, while improving the electrical and mechanical qualities of both materials.

Functionalized single- or multiwalled carbon nanotubes are spin-coated on copper foils and then heated and cooled, using the nanotubes themselves as the carbon source. Under heating, the functional carbon groups decompose into graphene, while the nanotubes partially split and form in-plane covalent bonds with the graphene, adding strength.  $\pi$ - $\pi$  stacking domains add more strength. The nanotubes can overlap, making the material a better conductor than standard CVD-grown graphene. The nanotubes effectively bridge the grain boundaries found in conventional graphene. The technique eliminates the traces of substrate on which later-separated sheets were deposited using epitaxy.

Stacks of a few layers have been proposed as a cost-effective and physically flexible replacement for indium tin oxide (ITO) used in displays and photovoltaic cells.

## 1.17 Applications

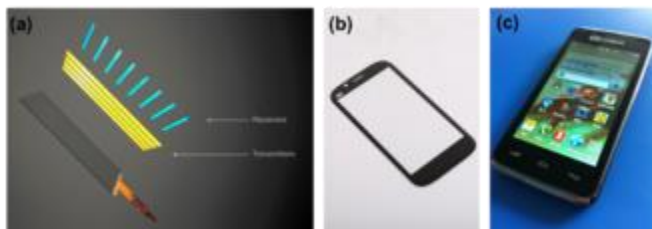


**Fig.1.9(a) The typical structure of a touch sensor in a touch panel. (Image courtesy of Synaptics, Incorporated.) (b) An actual example of 2D Carbon Graphene Material Co. Ltd's graphene transparent conductor-based touchscreen that is employed in (c) a commercial smartphone.**

## 1.18 Potential applications

Graphene is an extremely diverse material, and can be combined with other elements (including gases and metals) to produce different materials with various superior properties. Researchers all over the world continue to constantly investigate and patent graphene to learn its various properties and possible applications, which include:

- Batteries
- Transistors
- Computer chips
- Energy generation
- Super-capacitors
- DNA sequencing
- Water filters
- Antennas
- Touchscreens (for LCD or OLED displays)
- Solar cells
- Spintronics-related products

## 1.19 Graphene products

Several companies offer graphene and graphene based products. You may check our [list of graphene related companies](#) to find a company that offers the products you need.

In December 2011 [Vorbeck Materials](#) said that the [Siren anti-theft packaging device](#), which uses their graphene-based Vor-Ink circuitry (shown below) has started shipping - and this was the world's first commercially available product that is based on graphene.



**Fig. 1.10 Graphene Products**

Today there are several more graphene products on the market. The sport industry was an early adopter, and as early as 2013 HEAD started shipping graphene-enhanced tennis rackets (called YouTek Graphene Speed series). Today one can buy graphene-enhanced helmets, ski equipment and even Lacrosse gear.



**Fig.1.11 Tennis Racket**

Graphene has also entered the consumer electronics market - for example some of Huawei's flagship smartphones, use graphene film cooling technology for heat management purposes. Another high-profile company that adopts graphene is Ford - which is using graphene-reinforced foam covers for noisy components in its 2019 F-150 and Mustang cars. Ford uses graphene mixed with foam constituents, and the resulting parts are said to be 17% quieter, 20% stronger, and 30% more heat-resistant



**Fig.1.12 Smartphones**



An interesting market for graphene is the sensors market. In 2016 for example San Diego-based Nanomedical Diagnostics (now called Cardea) started shipping its graphene-based sensors and the AGILE R100 system which allows for real-time detection of small molecules. The graphene sensor offers faster sample processing, greater accuracy, portability and cost savings.



**Fig. 1.13 Graphene-based sensors**

## 1.20 Molybdenum diselenide (MoSe<sub>2</sub>)

**Molybdenum diselenide** (MoSe<sub>2</sub>) is an inorganic compound of molybdenum and selenium. Its structure is similar to that of MoS<sub>2</sub>. Compounds of this category are known as transition metal dichalcogenides, abbreviated TMDCs. These compounds, as the name suggests, are made up of a transition metals and elements of group 16 on the periodic table of the elements. Compared to MoS<sub>2</sub>, MoSe<sub>2</sub> exhibits higher electrical conductivity.

### 1.20.1 Structure

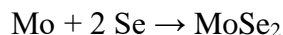
Like many TMDCs, MoSe<sub>2</sub> is a layered material with strong in-plane bonding and weak out-of-plane interactions. These interactions lead to exfoliation into two-dimensional layers of single unit cell thickness.

The most common form of these TMDCs have trilayers of molybdenum sandwiched between selenium ions causing a trigonal prismatic metal bonding coordination, but it is octahedral when the compound is exfoliated. The metal ion in these compounds is surrounded

by six  $\text{Se}^{2-}$  ions. The coordination geometry of the Mo is sometimes found as octahedral and trigonal prismatic.

### **1.20.2 Synthesis**

Synthesis of  $\text{MoSe}_2$  involves direct reaction of molybdenum and selenium in a sealed tube at high temperature. Chemical vapor transport with a halogen (usually bromine or iodine) is used to purify the compound at very low pressure (less than  $10^{-6}$  torr) and very high temperature (600–700 °C). It has to be heated very gradually to prevent explosion due to its strong exothermic reaction. Stoichiometric layers crystallize in a hexagonal structure as the sample cools. Excess selenium can be removed by sublimation under vacuum.<sup>[10]</sup> The synthesis reaction of  $\text{MoSe}_2$  is:



### **2D-MoSe<sub>2</sub>**

Single-crystal-thick layers of  $\text{MoSe}_2$  are produced by scotch tape exfoliation from bulk crystals or by chemical vapor deposition (CVD).

The electron mobility of 2D- $\text{MoSe}_2$  is significantly higher than that of 2D- $\text{MoS}_2$ . 2D  $\text{MoSe}_2$  adopts structures reminiscent of graphene, although the latter's electron mobility is thousands of times greater still. In contrast to graphene, 2D- $\text{MoSe}_2$  has a direct band gap, suggesting applications in transistors and photodetectors.

### **1.20.3 Natural occurrence**

Molybdenum(IV) selenide occurs in the nature as the extremely rare mineral drysdallite.

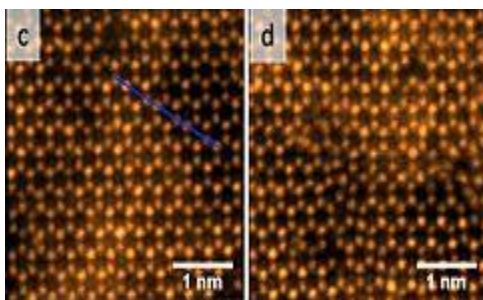


**Fig. 1.14 MoSe2 MicroStructure**

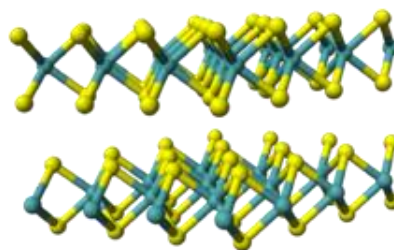




**Fig. 1.15 MoSe2 Structure**

**Table 1.1 Names**

<b>Table 1</b>
Names
<u>IUPAC name</u>
bis(selanylidene)molybdenum
<u>Other names</u>
molybdenum diselenide, molybdenumdiselenide, molybdenum selenide, diselanylidenemolybdenum, molybdenum(IV) selenide

**Table 1.2 Identifiers**

<u>CAS Number</u>	• <u>12058-18-3</u>
3D model ( <u>JSmol</u> )	• <u>Interactive image</u>
<u>ECHA InfoCard</u>	<u>100.031.831</u> 
<u>PubChem</u> CID	• <u>82894</u>

<a href="#">CompTox Dashboard (EPA)</a>	<ul style="list-style-type: none"> <li>• <a href="#">DTXSID4065234</a> </li> </ul>
	<ul style="list-style-type: none"> <li>• </li> </ul>

**Table 1.3 Properties**

<u>Chemical formula</u>	MoSe <sub>2</sub>
<u>Molar mass</u>	253.86 g/mol <sup>[2]</sup>
<u>Appearance</u>	crystalline solid
<u>Density</u>	6.90 g/cm <sup>3</sup> <sup>[2]</sup>
<u>Melting point</u>	>1200 °C
<u>Band gap</u>	~0.85 eV (indirect, bulk) ~1.5 eV (direct, monolayer)

**Table 1.4 Structure**

<u>Crystal structure</u>	hP6, space group P6 <sub>3</sub> /mmc, No 194 <sup>[5]</sup>
<u>Lattice constant</u>	$a = 0.3283$ nm, $c = 1.2918$ nm
<u>Coordination geometry</u>	Trigonal prismatic (Mo <sup>IV</sup> ) Pyramidal (Se <sup>2-</sup> )

## 1.21 HEXAGONAL BORON NITRIDE (HBN) POWDER

Hexagonal Boron Nitride is also called ‘White Graphite’ and has a crystal structure similar to Graphite. It is much superior to Graphite and its crystal structure provides good lubricating properties. It is available in powder form in different particle sizes as 70 nm, 150 nm, 0.5 microns, 1.5 microns and 5 microns.

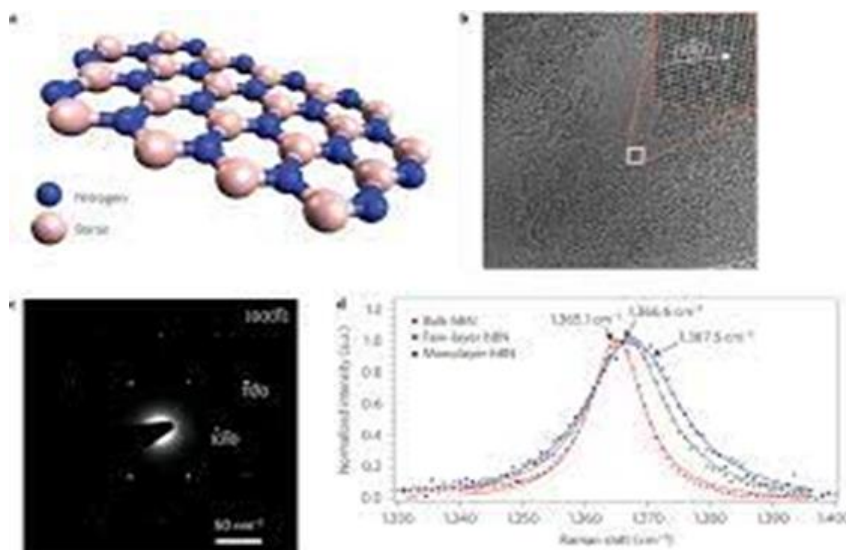


**Fig. 1.16 Structural characterization of hBN**

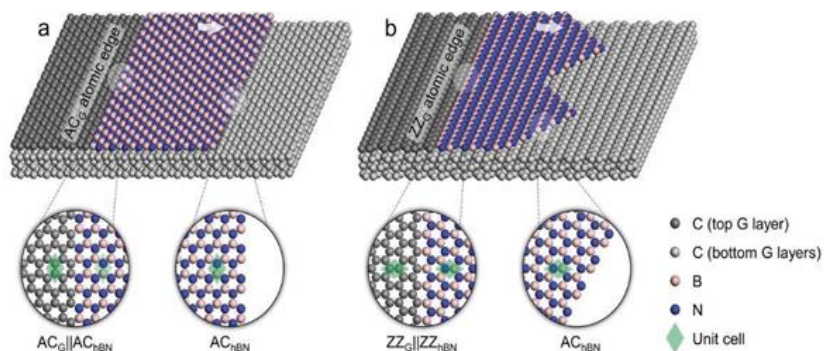


**Fig. 1.17 Graphene hBN Advancement Boosts Quantum Device Development**

### 1.21.1 Characteristic Of Hexagonal Boron Nitride Powder

- It has a low coefficient of friction at 0.5 to 0.70 and has excellent lubricating properties.
- It has good chemical inertness.
- It acts as an electric insulator.
- It is a good thermal conductor that leads to better heat dissipation.
- It shows stability at high temperatures - 1000° C in air, 1400° C in vacuum and 1800° C in inert gas.
- It has properties like low thermal expansion and low dielectric constant.
- It has high load-bearing properties.
- It is non-wetting and provides a strong resistance to chemical attacks. It cannot be wetted by glasses, salts and most metals.
- It is easily machinable in a hot-pressed state and complex shapes can be machined from the hot pressed structure.

### 1.21.2 Physical Properties Of Hexagonal Boron Nitride (HBN) Powder

The boron nitride can exist in different forms depending on the arrangement of the boron and the nitrogen atoms. This gives rise to various bulk properties of boron nitride. The hexagonal form is the most stable and soft among the polymers. Therefore, it is used as a lubricant and additive to cosmetic products.

### 1.21.3 Structural and Electronic Properties of BN

Boron nitride, BN, can exist in a variety of crystal structures, including hexagonal (h-BN) similar to the graphite structure, rhombohedral, hexagonal wurtzite (wz-BN), and cubic zincblende (zb-BN). The boron–nitrogen bond in BN is very strong, and that contributes in a major way to the large VB-to-CB energy gap  $E_g$ . Cubic zincblende BN is the most thermodynamically stable of the crystal structures. It can be produced in bulk form by a process that includes heating at 2000–3000 °C at high pressure, and thin films of zb-BN can be made by various processes. The bandgap of zb-BN has been measured as  $6.4 \pm 0.5$  eV (Chrenko, 1974) and as  $6.1 \pm 0.2$  eV (Miyata *et al.*, 1989). The less stable wz-BN is more difficult to produce and has an  $E_g$  value reported to be in the range 4.5–5.5 eV. The electronic levels of intrinsic defects and of impurities

in BN have been investigated in a few theoretical studies, but there has been rather little experimental investigation of such levels.

#### **1.21.4 Uses Of Hex Boron Nitride (HBN) Powder**

- As hBN powder has a thermal resistance and therefore it is used as an additive for high-temperature lubrication.
- The hBN powder is used as a lubricant additive and can be dispersed in lubricating oil, grease, water and solvents. When the hexagonal boron nitride powder is mixed with water and binders it can be applied as paint (lubricity coating).
- The hBN powder can be sprayed or sprinkled on hot surfaces to provide dry lubricity.
- The hBN has a high electric breakdown strength and resistivity. It is used as an electric insulator in electronics as a substrate for semiconductors, microwave transparent windows, seals, electrodes and as a catalyst in fuel cells and batteries. It can be used as a filler for insulation.
- It is a good thermal conductor and therefore it is used in different types of heat radiation material.
- As hBN shows chemical inertness it is used in the manufacture of crucibles, boats, molten metal carriage pipes pumps, thermocouple protection sheaths and lining of reaction vessels.
- Because of its high lubricity, it is used as a mold release agent for plastic injection and metal injection molds. An hBN coating is used in refractory molds for glass forming and Titanium forming.
- It is used in the glass manufacturing process due to its non-wetting properties.
- The powder due to its self-lubricating properties can be mixed with ceramics, alloys, resins, plastics, rubbers and more.
- As it has high-temperature stability it can be used in many aeronautic and space applications.
- It is used in the manufacture of paints, cosmetics, dental cement, pencil leads and more.

#### **Literature Review:**

**Zhenlu Sun et al** theoretically investigated the structural stability, electronic and optical of the sandwich graphene-MoSe<sub>2</sub>-graphene (G-MoSe<sub>2</sub>-G) heterostructure via the density functional theory (DFT). The simulation revealed that the relative movement of the layers along the plane

can hardly affect the electronic and optical properties, as well as the structural stability. However, both the vertical and biaxial strain applied to the sandwich heterostructure can significantly modify the band structure, which results in the change of electronic and optical properties. We elucidated the mechanism for the band tuning by examining the projected band structure and the charge transfer between graphene and MoSe<sub>2</sub> layers. In the meantime, the absorption peak at  $\sim 1.3$  nm shifted with the increase of the strain. We believe that the sandwich heterostructure can be of great interest for applications as optical modulators, sensors and photodetectors. **(Theoretical investigation on electronic and optical properties of the graphene-MoSe<sub>2</sub>-graphene sandwich heterostructure)**

**Zhang Nan** The thesis starts with the general overview of the properties of transition metal dichalcogenides monolayers and their heterostructures. This is followed by the detailed description experimental techniques which were used to characterize photo-response of heterostructures and their preparation. In chapter 3 the impact of photodoping on the interlayer exciton emission properties is presented. The photodoping is identified by the increasing (upon illumination) trion dissociation energy, accompanied by a characteristic change of the exciton/trion photoluminescence intensity ratio in MoSe<sub>2</sub>. At the same time, the photoluminescence intensity of the interlayer exciton decreases. This is accompanied by an enhancement of the combined PL intensity of the exciton and the Trion in MoSe<sub>2</sub>, showing that the interlayer charge transfer can be controlled by the doping level. This effect is persistent on a timescale of several hours, as long as the sample is maintained under vacuum. This indicates a mechanism involving laser induced desorption of molecules physisorbed on the surface of the heterostructure. This hypothesis is supported by the observed sensitivity of the photodoping rate on the excitation wavelength. The process of photodoping is much faster for higher energy photons. Chapter 4 presents the impact of the moiré pattern on the intralayer exciton spectrum in MoS<sub>2</sub>/MoSe<sub>2</sub> heterostructure. A moiré pattern forms in van der Waals stacks due to the weak interlayer interaction which allows the layers preserve their own lattice parameters. A small twist angle, or lattice mismatch between the layers, induces a periodic spatially varying potential. The relative orientation of the flakes in the investigated heterostructure has been determined using second harmonic generation spectroscopy. Experimental evidence is presented for the impact of the moiré pattern on the intralayer emission in a MoSe<sub>2</sub>/MoS<sub>2</sub> heterobilayer encapsulated in hexagonal boron nitride. The periodic in-plane potential results in a splitting of the MoSe<sub>2</sub>



exciton and trion in emission and which seen also in the absorption spectra of the exciton. The observed energy difference between the split peaks is fully consistent with theoretical predictions. Chapter 5 reports the impact of sample quality, and the possibility to generate valley polarization using magnetic field. Three types of structures are compared, namely, CVD grown and h-BN encapsulated MoSe<sub>2</sub>, together with MoSe<sub>2</sub>/MoS<sub>2</sub> heterostructure. The magneto-optical data suggest that the formation of moire pattern has negligible impact on the Landé g-factor of the intralayer excitonic transition. **(Electronic properties of MoS<sub>2</sub>/MoSe<sub>2</sub> van der Waals heterostructure.)**

**Jingang Wang, et al** In recent years, two-dimensional atomic-level thickness crystal materials have attracted widespread interest such as graphene, hexagonal boron nitride (h-BN), silicene, germanium, black phosphorus (BP), transition metal sulfides and so on. These graphene-like two-dimensional (2D) materials have a lot of excellent characteristics such as high specific surface area and high Young's modulus, and many potential applications in diverse areas such as photo-electricity, catalysts, and transistors. In this review, we introduced the synthesis, structure, properties, and applications of graphene, h-BN, and their heterostructures, especially focused on their mechanical, optical, thermal, electric, and magnetic properties. Finally, we present the outlooks and perspectives for these types of excellent 2D materials and their potential applications. **(Graphene, hexagonal boron nitride, and their heterostructures: properties and applications.)**

**Zhang, Qiang, et al** The van der Waals interaction in vertical heterostructures made of two-dimensional (2D) materials relaxes the requirement of lattice matching, therefore enabling great design flexibility to tailor novel 2D electronic systems. Here we report the successful growth of MoSe<sub>2</sub> on single-layer hexagonal boron nitride (hBN) on the Ru(0001) substrate using molecular beam epitaxy. Using scanning tunnelling microscopy and spectroscopy, we found that the quasi-particle bandgap of MoSe<sub>2</sub> on hBN/Ru is about 0.25 eV smaller than those on graphene or graphite substrates. We attribute this result to the strong interaction between hBN/Ru, which causes residual metallic screening from the substrate. In addition, the electronic structure and the work function of MoSe<sub>2</sub> are modulated electrostatically with an amplitude of 0.13 eV. Most interestingly, this electrostatic modulation is spatially in phase with the Moire' pattern of hBN on Ru(0001) whose surface also exhibits a work function modulation of the same amplitude.

## **(Bandgap renormalization and work function tuning in MoSe<sub>2</sub>/hBN/Ru(0001) heterostructures)**

**Jalal Azadmanjiri et al** Two-dimensional (2D) nanomaterials have recently gained interest due to their unique properties which their bulk counterparts do not exhibit. Several 2D nanomaterials have been developed till date, but particularly, transition metal dichalcogenides (TMDs) and graphene have attracted a considerable worldwide research interest due to their excellent properties. The possibility of forming 2D van der Waals (vdW) heterostructures have opened a new way for combining the meritorious properties of graphene and TMDs in a single unit. Due to alteration of Fermi level and Schottky barrier height, the 2D layered graphene/TMD vdW heterostructures could give rise to new properties which are not indigenous either to graphene or TMDs. In this article, we have focused on the recent advances in understanding the characteristics and behavior of 2D layered graphene/TMD heterostructures in various applications. In this context, we firstly discuss the electron transfer characteristics at the interfaces of graphene and TMD heterostructures. Tunable properties of these heterostructures by considering their different architectures are then evaluated. Thirdly, overview approaches in the synthesis of these heterostructures are illustrated. After that, the current conditions of applications of these heterostructures in energy storage, energy conversion, optoelectronic and sensing devices are discussed. The final section remarks the challenges and prospects of 2D vdW graphene and TMD heterostructures. **(Graphene-Supported 2D transition metal dichalcogenide van der waals heterostructures)**

## **References:**

1. *"graphene definition, meaning – what is graphene in the British English Dictionary & Thesaurus – Cambridge Dictionaries Online". [cambridge.org](http://cambridge.org).*
2. ^ Jump up to:<sup>a b c d e f g h i j k l m n o</sup> Geim, A. K.; Novoselov, K. S. (26 February 2007). "The rise of graphene". *Nature Materials*. **6** (3): 183–191. [arXiv:cond-mat/0702595](https://arxiv.org/abs/cond-mat/0702595). *Bibcode*:2007NatMa...6..183G. *doi*:10.1038/nmat1849. *PMID* 17330084. *S2CID* 14647602.

3. <sup>^</sup> Peres, N. M. R.; Ribeiro, R. M. (2009). "Focus on Graphene". *New Journal of Physics*. **11** (9): 095002. Bibcode:2009NJPh...11i5002P. doi:10.1088/1367-2630/11/9/095002.
4. <sup>^</sup> Jump up to:<sup>a b</sup> [1] "Carbon nanostructures for electromagnetic shielding applications", Mohammed Arif Poothanari, Sabu Thomas, et al., *Industrial Applications of Nanomaterials*, 2019. "Carbon nanostructures include various low-dimensional allotropes of carbon including carbon black (CB), carbon fiber, carbon nanotubes (CNTs), fullerene, and graphene."
5. <sup>^</sup> Zdetsis, Aristides D.; Economou, E. N. (23 July 2015). "A Pedestrian Approach to the Aromaticity of Graphene and Nanographene: Significance of Huckel's  $(4n + 2)\pi$  Electron Rule". *The Journal of Physical Chemistry C*. **119** (29): 16991–17003. doi:10.1021/acs.jpcc.5b04311.
6. <sup>^</sup> Jump up to:<sup>a b</sup> Harris, Peter (12 January 2018). "Transmission Electron Microscopy of Carbon: A Brief History". *C*. **4** (1): 4. doi:10.3390/c4010004.
7. <sup>^</sup> Li, Zhilin; Chen, Lianlian; Meng, Sheng; Guo, Liwei; Huang, Jiao; Liu, Yu; Wang, Wenjun; Chen, Xiaolong (2015). "Field and temperature dependence of intrinsic diamagnetism in graphene: Theory and experiment". *Phys. Rev. B*. **91** (9): 094429. Bibcode:2015PhRvB..91i4429L. doi:10.1103/PhysRevB.91.094429. S2CID 55246344.
8. <sup>^</sup> Jump up to:<sup>a b c d</sup> Nair, R. R.; Blake, P.; Grigorenko, A. N.; Novoselov, K. S.; Booth, T. J.; Stauber, T.; Peres, N. M. R.; Geim, A. K. (6 June 2008). "Fine Structure Constant Defines Visual Transparency of Graphene". *Science*. **320** (5881): 1308. arXiv:0803.3718. Bibcode:2008Sci...320.1308N. doi:10.1126/science.1156965. PMID 18388259. S2CID 3024573.
9. <sup>^</sup> Jump up to:<sup>a b c</sup> Zhu, Shou-En; Yuan, Shengjun; Janssen, G. C. A. M. (1 October 2014). "Optical transmittance of multilayer graphene". *EPL*. **108** (1): 17007. arXiv:1409.4664. Bibcode:2014EL....10817007Z. doi:10.1209/0295-5075/108/17007. S2CID 73626659.
10. <sup>^</sup> Jump up to:<sup>a b</sup> Lee, Changgu (2008). "Measurement of the Elastic Properties and Intrinsic Strength of Monolayer Graphene". *Science*. **321** (385): 385–

388. Bibcode:2008Sci...321..385L. doi:10.1126/science.1157996. PMID 18635798. S2CID 206512830.
11. ^ Jump up to:<sup>a</sup> <sup>b</sup> Cao, K. (2020). "Elastic straining of free-standing monolayer graphene". *Nature Communications*. **11** (284): 284. Bibcode:2020NatCo..11..284C. doi:10.1038/s41467-019-14130-0. PMC 6962388. PMID 31941941.
  12. <sup>^</sup> Boehm, H. P.; Clauss, A.; Fischer, G. O.; Hofmann, U. (July 1962). "Das Adsorptionsverhalten sehr dünner Kohlenstoff-Folien" [The adsorption behavior of very thin carbon foils]. *Zeitschrift für anorganische und allgemeine Chemie (in German)*. **316** (3–4): 119–127. doi:10.1002/zaac.19623160303.
  13. Xin, Na; Lourembam, James; Kumaravadivel, Piranavan (April 2023). "Giant magnetoresistance of Dirac plasma in high-mobility graphene". *Nature*. **616** (7956): 270–274. doi:10.1038/s41586-023-05807-0. PMC 10097601. PMID 37045919.
  14. Balandin, A. A.; Ghosh, Suchismita; Bao, Wenzhong; Calizo, Irene; Teweldebrhan, Desalegne; Miao, Feng; Lau, Chun Ning (20 February 2008). "Superior Thermal Conductivity of Single-Layer Graphene". *Nano Letters*. **8** (3): 902–907. Bibcode:2008NanoL...8..902B. doi:10.1021/nl0731872. PMID 18284217. S2CID 9310741.
  15. "2010 Nobel Physics Laureates" (PDF). *nobelprize.org*.
  16. Felix, Isaac M.; Pereira, Luiz Felipe C. (9 February 2018). "Thermal Conductivity of Graphene-hBN Superlattice Ribbons". *Scientific Reports*. **8** (1): 2737. Bibcode:2018NatSR...8.2737F. doi:10.1038/s41598-018-20997-8. PMC 5807325. PMID 29426893.
  17. Neto, A Castro; Peres, N. M. R.; Novoselov, K. S.; Geim, A. K.; Geim, A. K. (2009). "The electronic properties of graphene" (PDF). *Rev Mod Phys*. **81** (1): 109–162. arXiv:0709.1163. Bibcode:2009RvMP...81..109C. doi:10.1103/RevModPhys.81.109. hdl:10261/18097. S2CID 5650871. Archived from the original (PDF) on 15 November 2010
  18. Harris PJF (2012). "Hollow structures with bilayer graphene walls". *Carbon*. **50** (9): 3195–3199. doi:10.1016/j.carbon.2011.10.050.

## **VESTA**

### **2.1 Introduction**

VESTA is a 3D visualization program for structural models, volumetric data such as electron/nuclear densities, and crystal morphologies. Some of the novel features of VESTA are listed below.

- Deal with multiple structural models, volumetric data, and crystal morphologies in the same window.
- Support multiple tabs corresponding to files.
- Support multiple windows with more than two tabs in the same process.
- Deal with virtually unlimited number of objects such as atoms, bonds polyhedra, and polygons on isosurfaces (theoretical limit on 32bit operating system is 1,073,741,823)
- Support lattice transformation from conventional to non-conventional lattice by using matrix. The transformation matrix is also used to create superlattice and sublattice.
- Visualize interatomic distances and bond angles that are restrained in Rietveld analysis with RIETAN-FP.
- Transparent isosurfaces can be overlap with structural models.
- Isosurface can be colored on the basis of another physical quantity.
- Arithmetic operations among multiple volumetric data files.
- High quality smooth rendering of isosurfaces and sections.
- Export high-resolution graphic images exceeding Video card limitation.

VESTA runs on Windows, Mac OS X, and Linux. It is contributed free of charge for non-commercial users.

### **2.2 New features in VESTA**

- Visualization of crystal morphologies
- Superimposition of multiple structural models, volumetric data, and crystal faces on the same Graphic Area

- Visualization of isosurfaces with multiple levels
- An extended bond-search algorithm to allow more sophisticated search in complex molecules, cage-like structures, etc.
- Calculations of electron and nuclear densities from structure parameters
- Calculations of Patterson-function densities from structure parameters or volumetric data
- Integration of electron and nuclear densities by Voronoi tessellation
- Significant performance improvements in rendering of isosurfaces and calculation of slices
- Output information about principal axes and mean square displacements for anisotropic thermal motion
- Determination of the best plane for selected atoms
- Displaying labels of atoms
- Customization of styles per sites or bond types
- Customization of symmetry operations
- Improvements in inputting files with various formats
- Support of undo and redo in GUI operations

## 2.3 Circumstances behind the development of VESTA

VESTA is originated from two GLUT- and GLUI-based applications, VICS and VEND, developed by Dr. Ruben A. Dilanian and Dr. Fujio Izumi during 2001-2004. They saw the light of day at the end of 2002 and, since then, continued their growth to be used widely in a variety of studies. However, we never get full satisfaction from their usability and performance. First, the combined use of VICS and VEND to visualize both crystal and electronic structures via text files is rather troublesome; on-the-fly visualization of these two kinds of images is highly desired. Second, their graphical user interface (GUI) is not very user-friendly because they are based on the old-fashioned toolkits, GLUT and GLUI, which have been no longer upgraded. Above all things, they require large system resources and source codes written in C language lack scalability owing to unrefined programming.

At the end of June 2004, one of the main developer Dilanian leaved the project and both VICS and VEND became unlikely to continue its progress. Then I decided to create a new program

employing a modern C++ GUI framework wxWidgets. We at first upgraded VICS to VICS-II with a new state-of-art GUI and further integrated VICS-II and VEND into the next-generation 3D visualization system VESTA, adding new capabilities.

## 2.4 Basics:

### 2.4.1 Symmetry and Unit Cell

The Unit cell tab in the Edit Data dialog box is used to give lattice parameters and the symmetry of a structure.

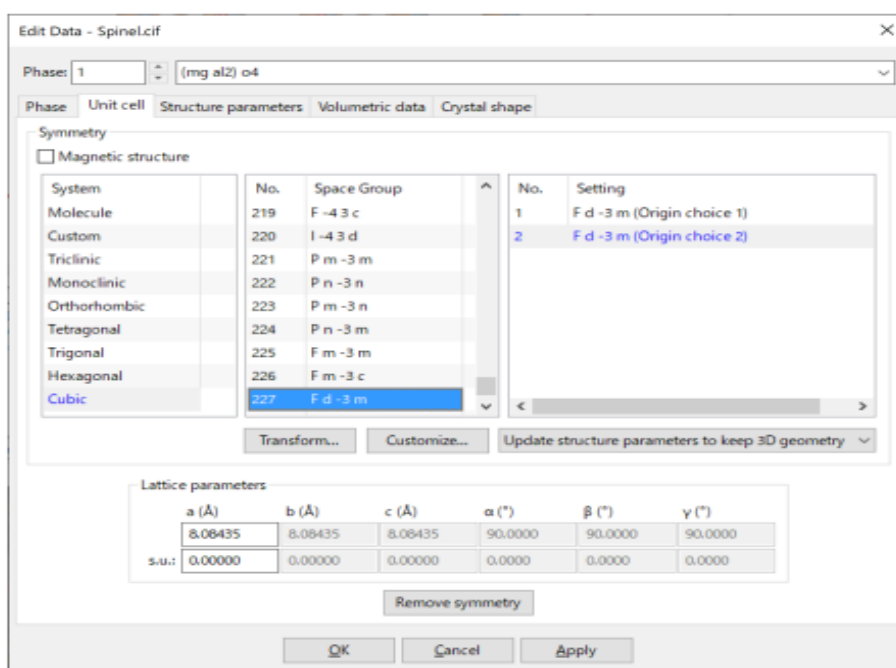


Fig. 2.1 Space group for structures

### 2.4.2 Crystal systems and space groups

#### Selection of crystal systems

The System list box is used to filter a list of space-group symbols in the Space group list box.

When an item in this list box is selected, only space groups belonging to the selected crystal system will be highlighted in the Space group list box. The following ten items are listed in the

System list box. There are 7 crystal systems in solids Geometry.

- Triclinic
- Monoclinic
- Orthorhombic
- Tetragonal
- Trigonal
- Hexagonal
- Cubic
- Rhombohedral

## **2.5 General features**

### **2.5.1 Cross-platform software**

VESTA runs on Windows, Mac OS X, and Linux.

### **2.5.2 Scalable**

VESTA allows us to deal with a practically unlimited number of objects as far as memory size goes.

### **2.5.3 Multiple windows and tabs**

VESTA supports multiple windows, each of which may contain multiple tabs corresponding to files.

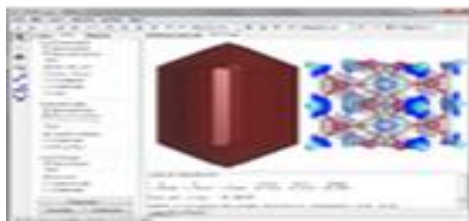


**Fig. 2.2 Interface for windows**



### 2.5.4 Smart ways of drawing boundary specification

Drawing boundaries for structural models can be changed in sophisticated ways similar to convoluting and reiterative convoluting spheres in ORTEP-III so that coordination polyhedra and molecules are not truncated. Cutoff planes in addition to x, y, z ranges can be used to specify drawing boundaries.

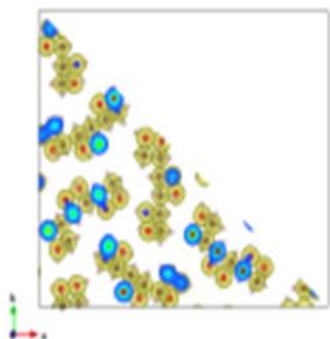


Fig.2.4

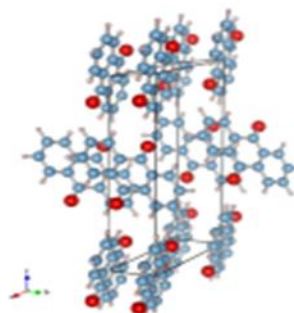


Fig. 2.5

## 2.6 Dealing with structural models

### 2.6.1 Visualization of structural model

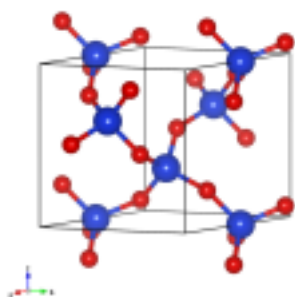


Fig. 2.6

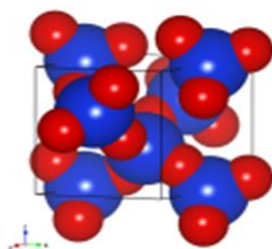


Fig. 2.7

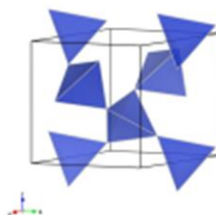


Fig. 2.8

## VESTA represents crystal structures as:

1. Ball & stick,
  2. Space filling,
  3. Polyhedral,
  4. Stick,
  5. wireframe
- me

Ball-and-stick , wireframe, and stick models can be overlapped with dotted surfaces corresponding to van der Waals radii. For ball-and-stick and polyhedral models, thermal displacement of atoms can be represented as ellipsoids.

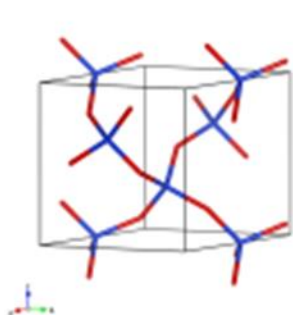


Fig. 2.9 Stick

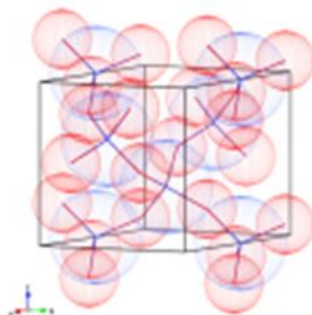


Fig. 2.10 firmware

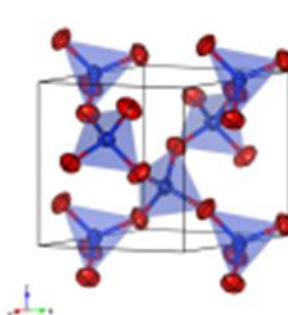
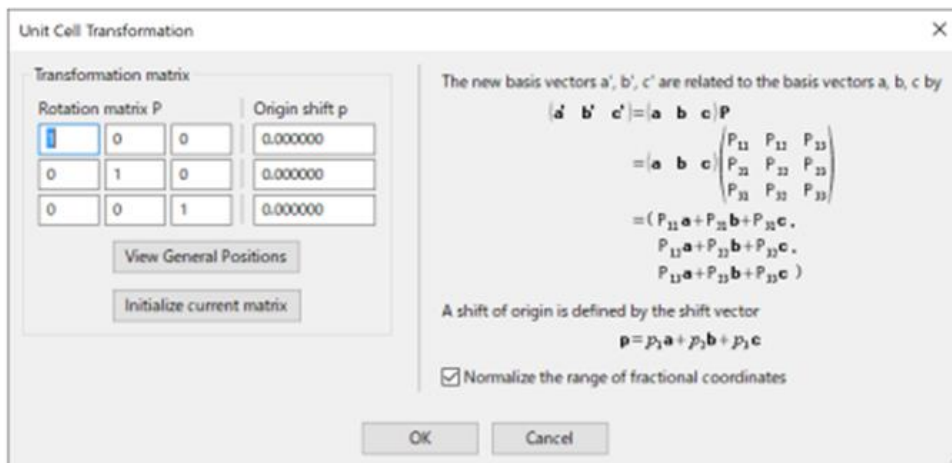


Fig. 2.11 Polyhedral

## 2.7 Functions in VESTA:

### 2.7.1 Transformation of Unit Cell

By Clicking the [Transform] Button opens the Unit Cell Transformation dialog box (Fig. 6.4). This dialog box allow you to transform crystal axes by specifying  $3 \times 3$  rotation matrix  $P$  and  $3 \times 1$  translation vector  $p$ . The [View general positions] button in the dialog box is used to open the Equivalent Positions dialog box to check the general equivalent positions and symmetry operations of the transformed unit cell (see 14.1). Clicking the [Initialize current matrix] button resets the transformation matrix to the identity matrix. Currently, this operation cannot be canceled. When option “Normalize the fractional coordinates” is checked, new atomic coordinates of the transformed unit cell will be normalized within a range of 0 to 1.



**Fig. 2.12 Unit Cell Transformation Dialog Box**

### 2.7.2 Creation of superstructures and substructures

The transformation matrix is also used to convert (primitive lattice)  $\rightleftharpoons$  (complex lattice) and to create superstructures and averaged substructures. To convert a structure, you have to select mode Update structure parameters to keep 3D geometry in the Unit cell tab of the Edit Data dialog box before opening the Unit Cell Transformation dialog box.

When the determinant of  $P$ ,  $\det(P)$  is larger than 1, the transformed unit-cell becomes larger than the original one, and when  $\det(P)$  is smaller than 1, the transformed unit-cell becomes smaller than the original one. In such cases, a dialog box appears to confirm whether you intend to change the unit cell volume (Fig. 6.7). Figure 6.7: A dialog box for confirmation of unit cell transformation. When a rotation matrix with  $\det(P) > 1$  is specified, or the transformed unit cell contains additional lattice points even when  $\det(P) = 1$ , a dialog box appears to ask you how to convert the structure (Fig. 6.8). There are the following three options:

- Add new equivalent positions to a list of symmetry operations
- Search atoms in the new unit cell and add them as new sites
- Do nothing

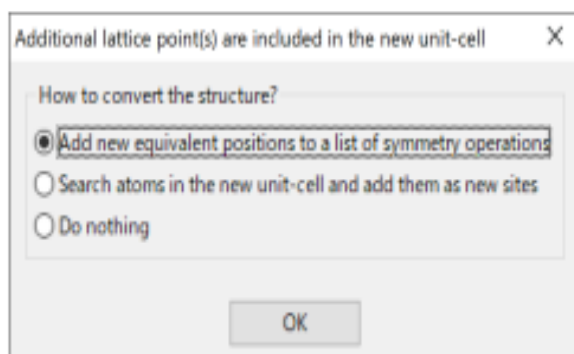


**Fig. 2.13 lattice points**

In the first and second options, the structural geometry of the original data will remain unchanged. On the other hand, on selection of the third option, some atoms in the new unit cell will be missing. On selection of the first option, a superstructure will be created by examining the following equation to find additional symmetry operations  $W'$  having a translational component in between  $(0, 0, 0)$  and  $(1, 1, 1)$

### **2.7.3 Magnetic Structures**

VESTA fully supports 1651 magnetic space groups. Check the “Magnetic structure” check box to use magnetic space groups. Then, the title of the Setting list box changes to BNS Setting, which shows a list of magnetic space groups for a selected space group. There are two types of notations of magnetic space groups: the Belov–Neronova–Smirnova (BNS) notation and the Opechowski–Guccione (OG) notation. VESTA uses the BNS notation because symmetry operations of the BNS notation are described with respect to the magnetic unit-cell with translational parts never exceeding 1. Atomic coordinates, displacement parameters, and occupancies of a magnetic structure are specified exactly the same way as conventional structure. Magnetic moments of atoms are specified in the Vectors dialog box.

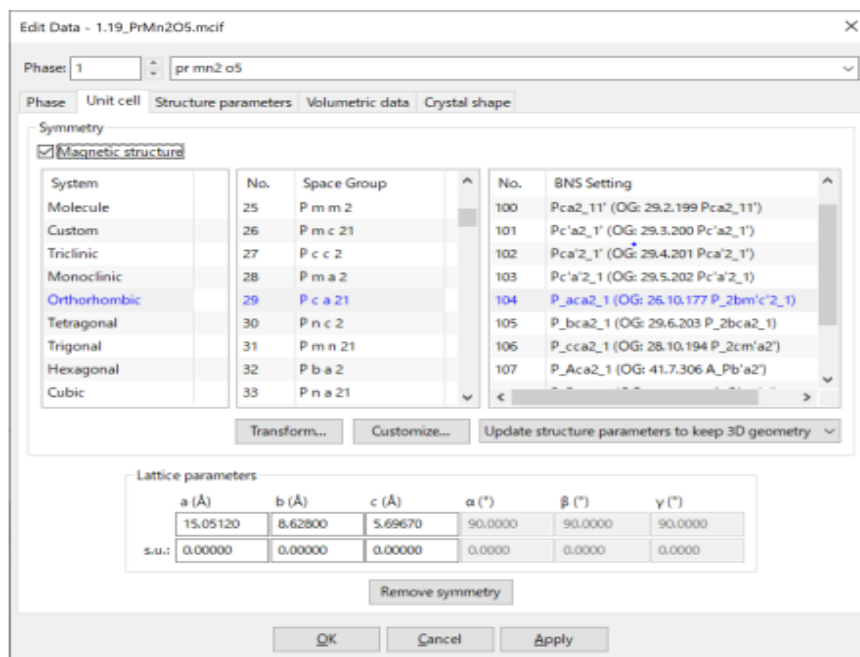
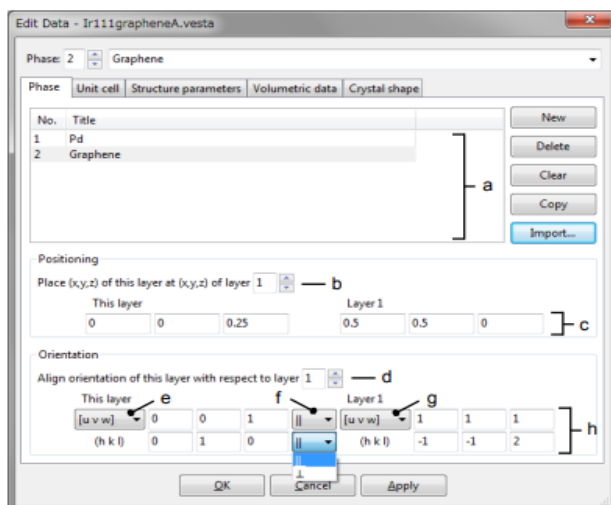


Fig. 2.14 Magnetic Structure Dialog Box

## 2.7.4 OVERLAYING MULTIPLE DATA

To display multiple-phase data in a single Graphics Area, set positioning and orientation of each phase after clicking the Phase tab in the Edit Data dialog box. The positioning and orientation of a phase are specified relative to another phase or the Cartesian coordinate system that is commonly used as internal representation of all phases. By default, the origin, (0, 0, 0), of a phase is placed at that of the internal coordinate system. The orientation of a phase is set such that the [1 0 0] axis of a phase is parallel to the x axis of the internal coordinate system with the [0 1 0] axis parallel to the x–y plane. To avoid the circular reference of phases, positioning and orientation must be set in descending order of the phase list.



**Fig. 2.15 Phase Dialog Box for overlaying Data**

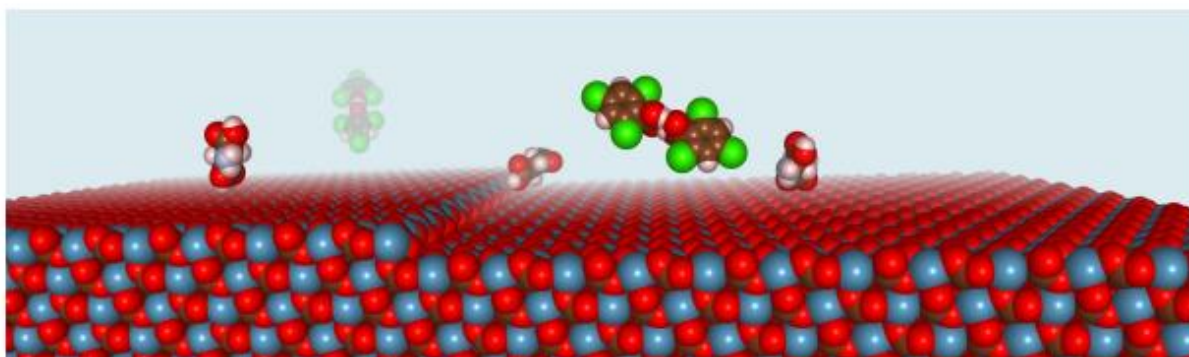


**Fig. 2.16 Molecules of L-aspartic acid and 2,4,6-trichlorobenzoic acid near a ( $10^{-14}$ ) surface of calcite ( $\text{CaCO}_3$ )**

### 2.7.5 Making Hetrojunction:

A **heterojunction** is an interface between two layers or regions of dissimilar semiconductors. These semiconducting materials have unequal band gaps as opposed to a homojunction. It is often advantageous to engineer the electronic energy bands in many solid-state device applications, including semiconductor lasers, solar cells and transistors. The combination of multiple heterojunctions together in a device is called a **heterostructure**, although the two terms are commonly used interchangeably. The requirement that each material be a semiconductor with unequal band gaps is somewhat loose, especially on small length scales, where electronic properties depend on spatial properties. A more modern definition of heterojunction is the

interface between any two solid-state materials, including crystalline and amorphous structures of metallic, insulating, fast ion conductor and semiconducting materials.

VESTA can be used to make heterojunctions of Materials and can visualize their structures.

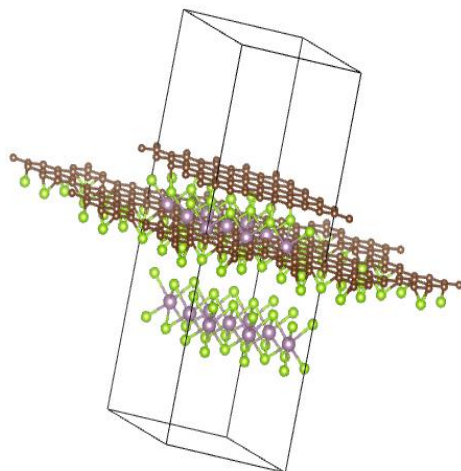


**Fig. 2.17 Graphene-MoSe2 Hetrojunction**

### **2.7.6 Making Heterostructures**

A heterostructure is defined as a semiconductor structure in which the chemical composition changes with position. The simplest heterostructure consists of a single heterojunction, which is an interface within a semiconductor crystal across which the chemical composition changes.

VESTA is a visualization program commonly used for crystal structures, but it can also be used for heterostructures. Heterostructures can be defined as a combination of different materials stacked together to create a new material with unique properties. VESTA can help visualize and analyze these heterostructures by displaying crystal structures, dislocations, and other related information. Additionally, VESTA can be used to calculate interfacial energies, which is important for understanding and predicting the behavior of heterostructures.

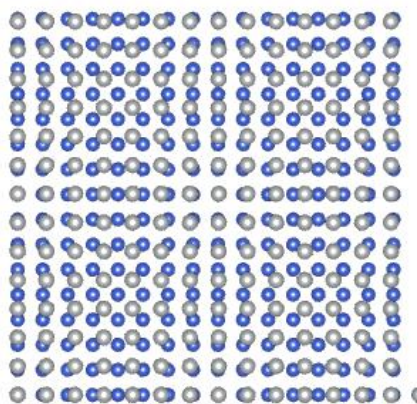


**Fig. 2.18**

Cu-Ag Hetrostructures

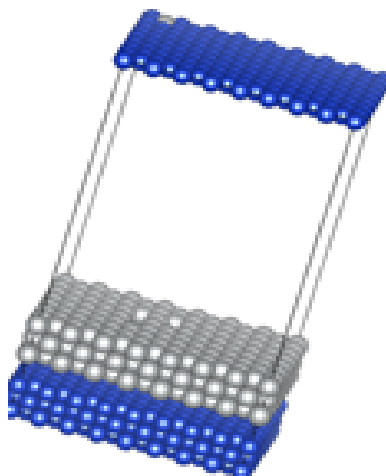


**Fig. 2.19**

### 2.7.7 Making Monolayers-Many Layers

A monolayer in crystal structures refers to a single layer of atoms or molecules that are arranged in a regular pattern on a substrate or surface. This term is often used in the context of thin films or surface coatings, where the thickness of the layer is typically only a few nanometers. Monolayers are useful for controlling the physical and chemical properties of surfaces, and they have applications in fields such as nanotechnology, materials science, and biotechnology.

A very simple monolayer for [001] orientation can be built by 1 x 1 x 5 supercell from the 1x1x1 unit cell of the corresponding bulk system. Make the c parameter of the crystal structure 5 times larger but keep the crystal itself to be 1 x 1 x 1 in size.

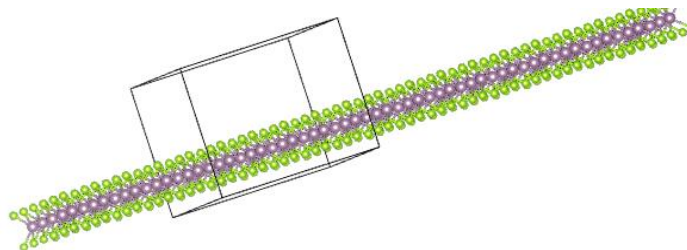


**Fig. 2.20 Monolayer of Mose2**



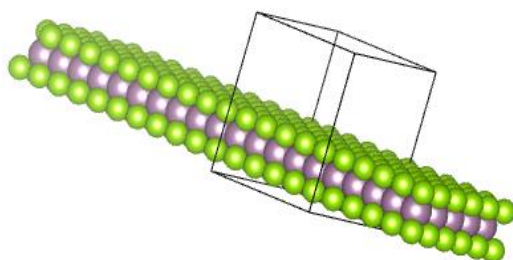


**Fig. 2.21**      **MoSe2 Monolayer**

### 2.7.8 Supercells

A supercell is a larger unit cell used to represent a crystal structure that contains more than one conventional unit cell. It is created by combining multiple conventional unit cells in a periodic arrangement. The purpose of using a supercell is to study the behavior of larger sections of a crystal structure, which may be useful in predicting the crystal's overall properties. Supercells are commonly used in computational studies of materials to simulate the behavior of crystals under different conditions. They can also be used to study defects, impurities, and other features that can affect the crystal's behavior.

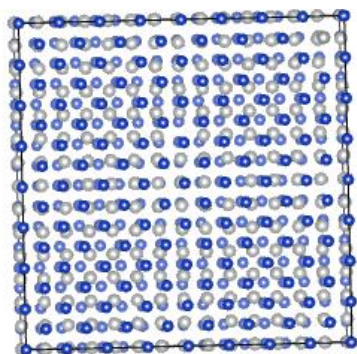


**Fig. 2.22**      **Supercell of CU**

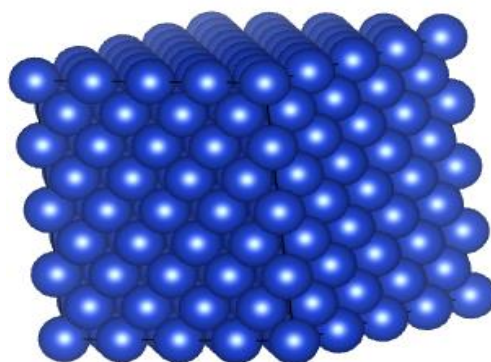


**Fig. 2.23**

### 2.7.9 Nanorods

Nanorods are tiny, rod-shaped structures that are only a few nanometers in diameter and several micrometers in length. They are often used in materials science and nanotechnology research due to their unique optical, electronic, and mechanical properties. In crystal structures, nanorods can be formed from a variety of materials, including metals, semiconductors, and polymers. They are

typically grown using a process known as solution synthesis, where a precursor solution is used to control the size, shape, and orientation of the nanorods. The resulting nanorods can be used in a wide range of applications, including solar cells, sensors, and electronic devices.

## **2.8 Display crystallographic information**

Selection of objects (atoms, bonds, and coordination polyhedra) by clicking with a mouse provides us with a variety of crystallographic information:

1. fractional coordinates,
2. symmetry operations and translation vectors,
3. site multiplicities, Wyckoff letters, and site symmetry,
4. information about principal axes and mean square displacements for anisotropic thermal motion
5. interatomic distances, bond angles, and torsion angles,
6. information about coordination polyhedra including volumes, Baur's distortion indices, quadratic elongations, bond angle variances, bond valence sums of central metals, and bond lengths expected from bond valence parameters.

## **2.9 Lattice transformation**

VESTA has a feature to convert general equivalent positions in a conventional setting into those in a non-conventional one with a transformation matrix, which is also used for (primitive lattice)-(complex lattice) conversions and for creating superstructures. Translucent isosurfaces can be overlapped with a structural model.

## **2.10 Vectors on atoms**

Vectors (arrows) showing magnetic moments or directions of static displacements can be attached to atoms.

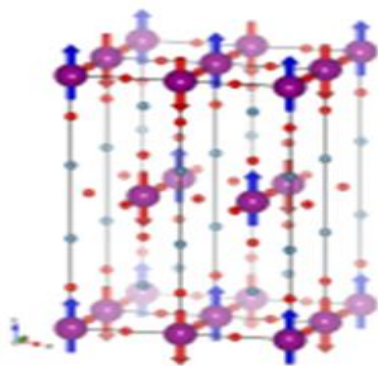


**Fig. 2.24 vector display**

## 2.11 Dealing with volumetric data:

The Volumetric data frame box in the Style tab of the Side Panel contains frequently used tools to control representation of volumetric data. The same options can also be used by selecting the “Volumetric Data” item under the “Objects” menu. This frame box is disabled for data containing no volumetric ones.

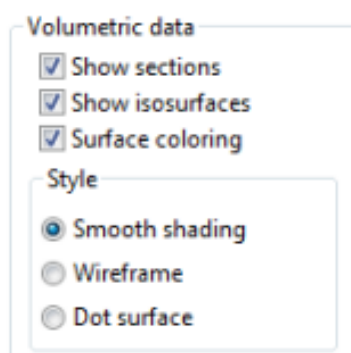


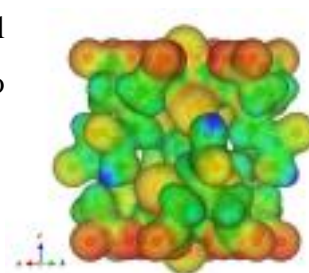
**Fig. 2.25 Volumetric Data options**

## 2.12 Visualization of volumetric data

Isosurfaces are represented as smooth-shaded polygons, wireframes, and dot surfaces. Physical quantities, e.g., wave functions and nuclear densities, having both positive and negative values can be expressed by isosurfaces with two different colors.

## 2.13 Surface coloring

VESTA has an attractive feature to colorize isosurfaces, whose typical application is to colorize isosurfaces of electron densities according to electrostatic potentials.



## 2.14 Peak search

Peak values and positions in 3D pixel data can be listed in Text Area.

## 2.15 Display lattice planes

Lattice planes with variable opacities can be inserted. For 3D pixel data, both boundary sections and lattice planes are colorized on the basis of numerical values on them.

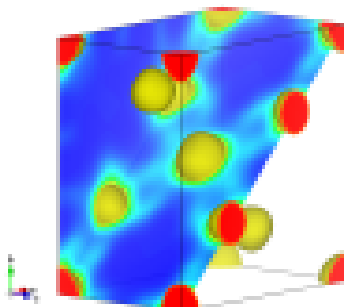


**Fig.2.26 Lattice Planes**

## 2.16 2D color & contour map

With a 2D Data Display window, 2D distribution of a physical quantity on a lattice plane can be visualized as a colored map with contour lines or Bird's-eye view.

## 2.17 Main Features:

### 2.17.1 Visualization of Crystal Morphologies

Crystal morphologies can be drawn by inputting Miller indices of faces.

### 2.17.2 Collaboration with external programs

## ORFFE

The "Geometrical Parameters" dialog box lists interatomic distances and bond angles recorded in \*.ffe output by ORFFE. On selection of a bond (2 atoms) or a bond angle (3 atoms) in this dialog box, the corresponding object in a ball-and-stick model is highlighted, and vice versa.

### 2.17.3 STRUCTURE TIDY

STRUCTURE TIDY allows us to standardize crystal-structure data and transform the current unit cell to a Niggli-reduced cell.

### 2.17.4 RIETAN-FP

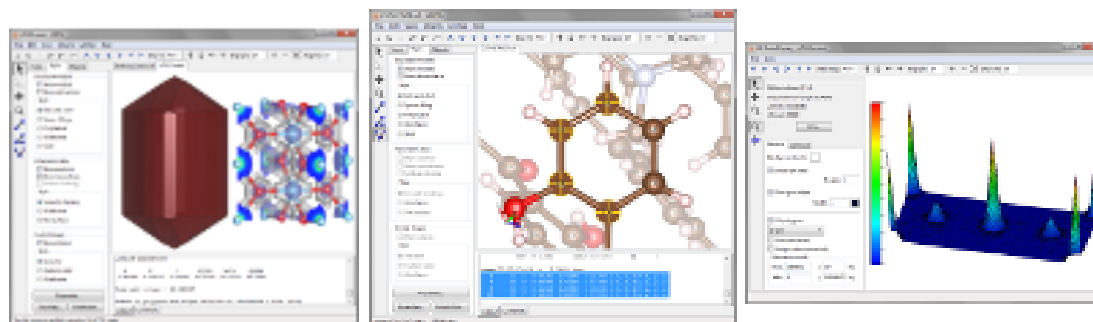
Powder diffraction patterns can be simulated with RIETAN-FP. On selection of the "Powder Diffraction Pattern..." menu, a series of procedures, i.e., generation of an input file, \*.ins, for RIETAN-FP, execution of RIETAN-FP, and graphic representation of the resulting data in file, \*.itx, with a graphing program such as Igor Pro and gnuplot, are executed by VESTA as if they were implemented in VESTA.

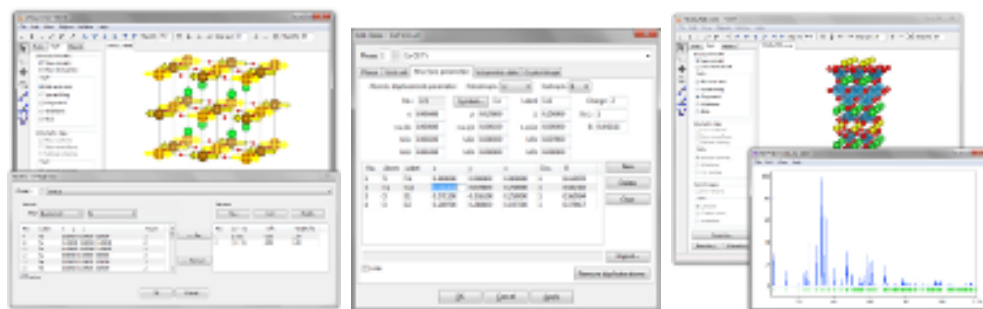
### 2.17.5 MADEL

VESTA utilizes an external program, MADEL, to calculate electrostatic site potentials and the Madelung energy in a crystal by the Fourier method.

## 2.18 Screenshots

### Windows





## 2.19 Crystal structure

Chibaite contains natural gas molecules such as methane, ethane, propane, and 2-methyl-propane (isobutane) within the cage-like silica framework. The framework topology of chibaite is isostructural with the structure-II gas hydrates.

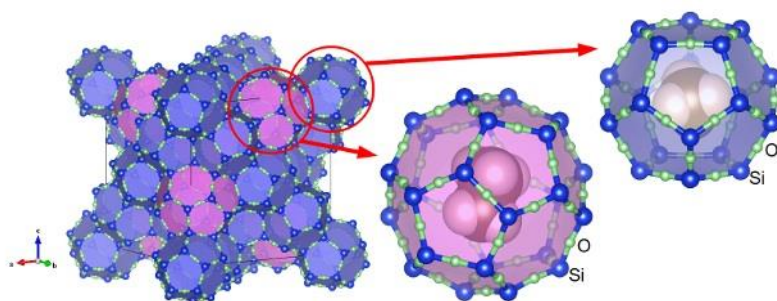


**Fig. 2.27** Crystal structure of chibaite

## Chapter no.3 Results and Discussion:

In our Project “Build Many Layer Graphene-MoSe<sub>2</sub>-hBN heterojunction with LatticeMixer and VESTA” we need to draw layers of our given material. First, We make a structure of Graphene in VESTA. Lattice Parameters of Graphene molecule are  $a = 2.47 \text{ \AA}$ ,  $b = 2.47 \text{ \AA}$ ,  $c = 7.80 \text{ \AA}$ ,  $\alpha = 90^\circ$ ,  $\beta = 90^\circ$ ,  $\gamma = 120^\circ$  Volume =  $41.14 \text{ \AA}^3$ . Space Group for Graphene is 194 with symbol  $P6_3/mmc$  Crystal system is Hexagonal. Atomic Positions of C atoms in Graphene are also given. For first C 0, 0, 1/4 for 2<sup>nd</sup> C positions are 1/3, 2/3, 1/4.[1] The Graphene structure is given below [2]

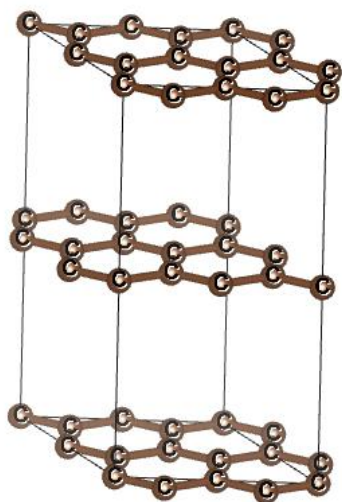


Fig. 3.1 Graphene Structure

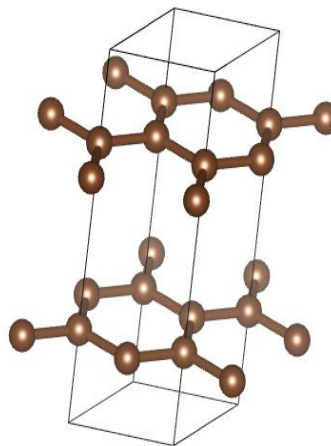
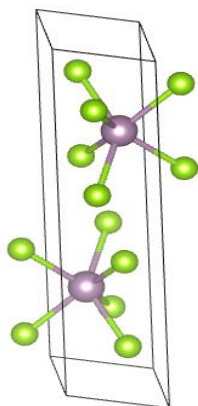


Fig. 3.2 Graphene 2-D Structure

2nd we make a structure of MoSe<sub>2</sub> in VESTA. Crystal system of MoSe<sub>2</sub> is Hexagonal. Space Group for MoSe<sub>2</sub> is 194 with symbol  $P6_3/mmc$ . Lattice Parameters for MoSe<sub>2</sub> are  $a = 3.32 \text{ \AA}$ ,  $b = 3.32 \text{ \AA}$ ,  $c = 13.54 \text{ \AA}$ ,  $\alpha = 90^\circ$ ,  $\beta = 90^\circ$ ,  $\gamma = 120^\circ$  volume is  $129.45 \text{ \AA}^3$ . Atomic Position for Mo and Se are also given. For Mo positions are 2/3, 1/3, 3/4 for Se positions are 1/3, 2/3, 0.8722222.[3] Structure of MoSe<sub>2</sub> is given below[4]



**Fig. 3.3 MoSe2 Structure**



**Fig. 3.4**

3rd, hBN is a hexagonal BN structure. We make a structure of hBN in VESTA by using Lattice parameters  $a = 2.51 \text{ \AA}$ ,  $b = 2.51 \text{ \AA}$ ,  $c = 7.71 \text{ \AA}$ ,  $\alpha = 90^\circ$ ,  $\beta = 90^\circ$ ,  $\gamma = 120^\circ$  volume is  $42.13 \text{ \AA}^3$ . Crystal system is Hexagonal. Space Group for MoSe2 is 194 with symbol  $P6_3/mmc$ . Atomic Positions for B and N are  $1/3 \ 2/3 \ 1/4$  and  $1/3 \ 2/3 \ 3/4$  respectively[5]. The structure of hBN is given below[6]

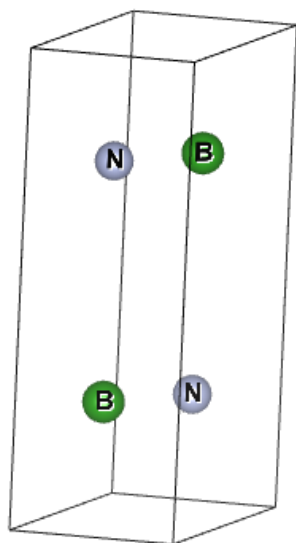


**Fig. 3.5 hBN structures**

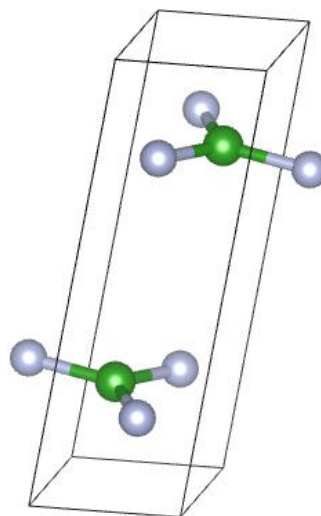


**Fig. 3.6**



Our next step is create Layers of Graphene-Mose2-hBN layers. For this we use LatticeMixer to make hetrostructure of Graphene-Mose2-hBN . LatticeMixer will mix the lattices of Graphene, MoSe2 and hBN . We will create many hetrojunction of our given Material. We can create many hetrojunctions of Graphene-MoSe2 by using LatticeMixer. LatticeMixer will give percentage of mixes of lattice atoms of Graphene-MoSe2. We can use 2 layers & 1 layer of Graphene & MoSe2 to make hetrojunctions. Here in our Project we use 1 layer of Graphene & MoSe2. As below

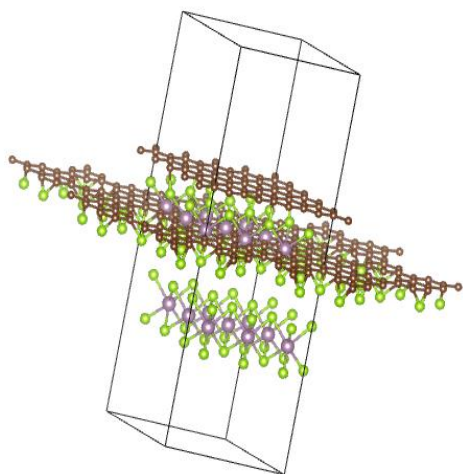


**Fig. 3.7 Graphene-MoSe2 using  
2 layers of each**

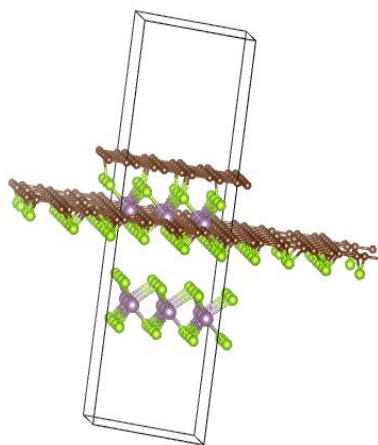


**Fig. 3.8 Graphene-MoSe2 using  
1 layer of each**

Hetrostructures Graphene-MoSe2 using 2 layers & 1 layer look like same when we open the hetrostructures of these in VESTA Software.

Now our last step is to mix lattice of Graphene-MoSe2-hBN in LatticeMixer. We can choose different structures of Graphene-MoSe2-hBN hetrojunctions. Maximum percentage of latticemixer is best to choose. Here is the structure.

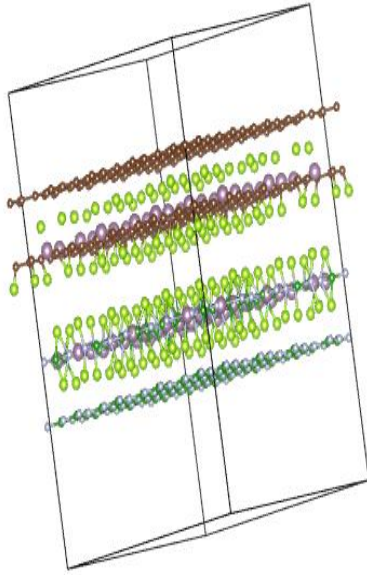


**Fig. 3.9 Graphene-MoSe2-hBN layers**

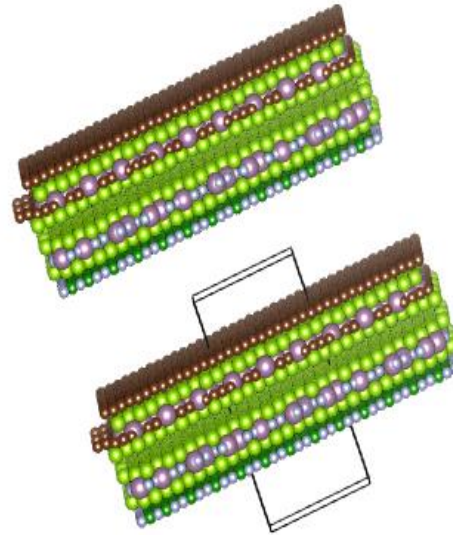


**Fig. 3.10 Many layers creating vacuum in z-axis**

## References:

1. Hattab, Hichem, Alpha T. N'Diaye, Dirk Wall, Claudius Klein, Giriraj Jnawali, Johann Coraux, Carsten Busse et al. "Interplay of wrinkles, strain, and lattice parameter in graphene on iridium." *Nano letters* 12, no. 2 (2012): 678-682.
2. Schumann, Timo, Martin Dubsclaff, Myriano H. Oliveira Jr, Michael Hanke, J. Marcelo J. Lopes, and Henning Riechert. "Effect of buffer layer coupling on the lattice parameter of epitaxial graphene on SiC (0001)." *Physical Review B* 90, no. 4 (2014): 041403.
3. James, Philip B., and M. T. Lavik. "The crystal structure of MoSe2." *Acta Crystallographica* 16, no. 11 (1963): 1183-1183.
4. Miller, Aaron M., Danielle M. Hamann, Erik C. Hadland, and David C. Johnson. "Investigating the Formation of MoSe2 and TiSe2 Films from Artificially Layered Precursors." *Inorganic Chemistry* 59, no. 17 (2020): 12536-12544.
5. Xu, Bin, Meizhe Lv, Xiaohong Fan, Wen Zhang, Yong Xu, and Tongguang Zhai. "Lattice parameters of hexagonal and cubic boron nitrides at high temperature and high pressure." *Integrated Ferroelectrics* 162, no. 1 (2015): 85-93.
6. Kurdyumov, A. V., V. L. Solozhenko, and W. B. Zelyavski. "Lattice parameters of boron nitride polymorphous modifications as a function of their crystal-structure perfection." *Journal of applied crystallography* 28, no. 5 (1995): 540-545.

## Chapter no.4      Conclusion:

In our Project” **Build Many Layer Graphene-MoSe<sub>2</sub>-hBN heterojunction with LatticeMixer and VESTA**” we made many layers of **Graphene-MoSe<sub>2</sub>-hBN** . We can identify and calculate the atomic distance of different atoms of Graphen-MoSe<sub>2</sub> or MoSe<sub>2</sub>-hBN . We can calculate the angle, Dihedral angle and Interfacial angle of different atoms of a crystal.

Heterostuctures of Different crystals give information about their physical, Electric, Magnetic and Dielectric Properties. By Mixing lattices of different crystals, the properties of crystals may change.

We can get different results by changing properties of crystals by mixing their lattices or hetrojunctions. A material is made efficient for its usage and applications in the field of science and Technology in our modern world.

In future, we can explore the properties of materials by making their hetrojunctions. We can study the Nano materials and their potential applications in the field of science and technology. We can study the properties of Nano materials e.g Electric, Magnetic, Dielectric and Optical Properties by making their hetrojunction as a Research area. We can explore and define crystal systems of different crystals to study the Nano materials.